PTEN neddylation aggravates CDK4/6 inhibitor resistance in breast cancer

Fan Liu [1,2,5], Weixiao Liu [1,2,5], Yawen Tan [3,5], Yaxin Shang [1], Sihui Ling [1], Xiaokun Jiang [4], Zhen Zhang [4], Shiyao Sun [3], Ping Xie [1,2,*]

1 Department of Cell Biology, Beijing Key Laboratory of Cancer Invasion and Metastasis Research, Capital Medical University, Beijing 100069, China;

2 Beijing lnstitute of Hepatology, Beijing Youan Hospital, Capital Medical University, Beijing 100069, China

3 Department of Breast and Thyroid Surgery, The Second People's Hospital of Shenzhen, Shenzhen, Guangdong 518035, China;

4 Department of Neurosurgery, Shandong Provincial Hospital affiliated to Shandong First Medical University, Jinan, Shandong 250021, China

5 These authors contributed equally: Fan Liu, Weixiao Liu, Yawen Tan

*Correspondence: Ping Xie (xiep@ccmu.edu.cn)

ABSTRACT

The gradual emergence of a novel therapeutic approach lies in the restoration of tumor suppressive machinery, specifically targeting PTEN. Protein neddylation modification contributes to PTEN inactivation and fuels breast cancer progression. Here, we highlight elevated level of PTEN neddylation is markedly associated with resistance against Palbociclib, a CDK4/6 inhibitor used in HR+/HER2- breast cancer patients. Strikingly, we identified a potent inhibitor of PTEN neddylation which could

obviously re-sensitized Palbociclib-therapy-resistant breast cancer. Mechanistically, PTEN neddylation activates the PI3K/Akt signaling pathway, and more importantly, it stabilizes JUND by disrupting the interplay with its E3 ubiquitin ligase, ITCH. Therefore, the enhanced stability of JUND activates the AP-1/MAPK signaling pathway, resulting in the release of cytokines and chemokines, in turn, reprograming the tumor microenvironment, contributing to drug resistance, tumor recurrence and metastasis. This novel insight underscores the potential of targeting PTEN neddylation as a promising strategy for restoring the activity of key tumor suppressor and overcoming resistance in breast cancer therapy.

INTRODUCTION

Breast cancer is a heterogeneous disease with multiple intrinsic tumor subtypes. Hormone receptor-positive (HR+) and human epidermal growth factor receptor 2-negative (HER2-) breast cancer subtype accounts for 70% of breast cancers patients [1, 2]. Endocrine therapy (ET) is the mainstay of systemic treatment, which effectively reduces the risk of recurrence and mortality [3]. Recently, in order to achieve better treatment outcomes for metastatic cancer patients, the combination of Cyclin D-dependent Kinases 4 and 6 inhibitors (CDK4/6i), Palbociclib, Ribociclib and Abemaciclib with ET has been approved by FDA for the treatment of patients with advanced HR+/HER2- breast cancer. In HR+/HER2- breast cancer, estrogen induces the activation of Cyclin D-CDK4/6 complex, resulting phosphorylate retinoblastoma gene (Rb), then promotes the cell cycle from the G1 mitosis phase to the S phase. Therefore, CDK4/6 inhibitors restore the cell cycle and block cell

proliferation by selectively inhibiting CDK4/6 [4, 5]. Palbociclib is primarily used to treat late-stage or metastatic HR+/HER2- breast cancer. Additionally, Palbociclib is also utilized in the adjuvant treatment of early breast cancer. Even though the great majority of patients with advanced disease have benefited from this combination with improved survival, resistance to CDK4/6i remains a significant unmet clinical challenge [6-8].

Over-activated PI3K/Akt signaling pathway is prominent as cancers become resistant to CDK4/6 inhibitors by Cyclin D1 upregulation along with CDK2-dependent Rb phosphorylation and S-phase entry [9-11]. However, although PI3K inhibitors could prevent resistance to CDK4/6 inhibitors, they failed to re-sensitize cells once resistance had been acquired [10, 12]. PTEN (phosphatase and tension homologue deleted from chromosome 10) is a well-known negative regulator of the PI3K signaling pathway and governing fundamental cellular processes [13-16]. Notably, PTEN loss is considered as a bona fide mechanism of resistance to CDK4/6 inhibitors. Loss of PTEN increases PI3K/Akt activity and increases activity of CDK4/6 [17-19]. Therefore, targeting the restoration of PTEN tumor suppressor activity has been considered as an “Achilles heel” for cancer , which may be a more effective approach to combat resistance to CDK4/6 inhibitors [20-22]. Besides, additional role of PTEN in acquired CDK4/6 inhibitors resistance remains elusive.

Nedd8 is a ubiquitin-like protein that is covalently conjugated to substrates in a manner similar to ubiquitin [23, 24]. Overactive neddylation has been indicated to be closely correlated with cancer development [25-27]. High levels of PTEN neddylation,

which enhances the activity of the PI3K/Akt pathway, promotes PTEN nuclear import and accelerates tumor proliferation and invasion [28, 29]. Here, we showed that PTEN neddylation influenced CDK4/6 inhibitor resistance in HR+/HER2- breast cancer by promoting MAPK/AP-1 pathway activation and reshaping the tumor microenvironment. More importantly, we identified Echinacoside (ECH), a natural phenylethanoid glycoside in *Echinacea angustifolia* DC, as a natural and potent PTEN neddylation inhibitor. Combined treatment of ECH therapeutically blunted Palbociclib resistance and enhanced drug sensitivity in HR+/HER2- breast cancer. Our findings unravel an innovative therapeutic strategy to limit cancer drug resistance through PTEN reactivation by blocking neddylation modification.

RESULTS

High PTEN neddylation levels associated with lack of response to Palbociclib in HR+/HER2- breast cancer

Our previous study indicates that PTEN neddylation positively correlates with the progression of human breast cancer [28]. Firstly, we confirmed that PTEN neddylation was significantly increased in breast cancer tissues (tumor n=80, adjacent n=80) and high PTEN neddylation accompanied poor prognosis (Figure 1A and 1B). Compared with different types of breast cancer, PTEN neddylation was upregulated in all sub-types, especially in HR+/HER2- type (Figure 1C). PTEN loss of function induces PI3K/Akt pathway activation has been linked to the progression of CDK4/6i resistance in HR+/HER2- breast cancer [17]. Since Palbociclib is mainly used for the

treatment of advanced breast cancer patients, it is hard to obtain tumors that have recurred *in situ* through clinical surgery. PTEN neddylation was detected in Palbociclib resistance breast cancer patient with liver metastasis. This patient developed resistance after two years of treatment with Palbociclib and subsequent liver metastasis (Figure S1A-S1C). Significantly, PTEN neddylation rather than PTEN was much higher in metastasis tumor with lack of response to Palbociclib than in *in situ* tumor with no Palbociclib treatment (Figure 1D). Next, we monitored MMTV-*PyMT* (C57BL/6J background) mice starting 91 days after birth, which is when the mice began to spontaneously develop breast tumors . Resistance to Palbociclib was generated from MMTV-*PyMT* mice after prolonged drug exposure (Figure 1E and 1F). The tumor weight and volume were obviously lack of response to Palbociclib (Figure 1G and 1H) and high level of PTEN neddylation was detected in Palbociclib resistant breast tumors, while the expression of PTEN was unobviously changed (Figure 1I). Simultaneously, the *in vivo* neddylation assay also demonstrated an augmentation of PTEN neddylation in breast cancer tissues that were derived from MMTV-*PyMT* mice (Figure 1J). The IC50 of those cells was detected to confirm the generation of Palbociclib resistance mouse model (Figure 1K). Taken together, our findings revealed that PTEN neddylation exhibited elevated levels in Palbociclib resistant breast cancer.

High protein level of XIAP enhances the PTEN neddylation in Palbociclib resistant breast cancer

According the above data, we hypothesize that PTEN neddylation modification plays a role in resistance to Palbociclib, but the underlying mechanism remains unclear. Then, acquired Palbociclib resistant HR+ breast cancer cell lines (MCF-7-PR) were established. Compared with the parental cells, the Palbociclib resistant cells could pass G1/S checkpoints (Figure 2A). Dose-response curves showed that MCF-7-PR was significantly more resistant to Palbociclib than the parental cells (MCF-7-PS) (Figure 2B). Palbociclib treatment also abolished colony formation in parental cells, but not in resistance cells (Figure 2C). Furthermore, high level of PTEN neddylation was also existed in acquired Palbociclib resistant breast cancer cells (Figure 2D). Compared with other drugs resistant breast cancer cells, including MCF-7 sublines resistant to doxorubicin (MCF-7/ADR), cisplatin (MCF-7/DDP) and paclitaxel (MCF-7/PTX), PTEN neddylation was specifically upregulated in acquired Palbociclib resistant breast cancer cells (Figure 2E). Next, we generated early adaptative resistance to CDK4/6 inhibition cell model in MCF-7. Palbociclib inhibited Rb phosphorylation after 48 hours treatment, but Rb phosphorylation returned when continuous exposure to Palbociclib over 96 hours, which indicates that there is an early adaptative Palbociclib resistance has occurred (Figure 2F). Our data showed that PTEN neddylation was also higher in Palbociclib early adaptative resistant cells than the parental cells (Figure 2G, left pannels). However, in T98G cells, which are ER negative glioma cells and less sensitive to Palbociclib [30], no obvious change of PTEN neddylation was detected (Figure 2G, right pannels).

Then, we intended to explore the mechanism of high PTEN neddylation in Palbociclib resistance breast cancer. Of note, our data revealed that XIAP, the neddylation E3 ligase of PTEN, was upregulated in MCF-7-PR breast cancer cells, while no significant changes were observed in E1-UBA3, E2-Ubc12, and Nedd8 (Figure 2H). The increased XIAP enhanced the interaction with PTEN in early adaptative Palbociclib resistantand acquired Palbociclib resistant breast cancer cell lines (Figure 2I-2K). Taken together, our data indicate that high levels of PTEN neddylation are associated with Palbociclib-resistant breast cancer tumors. Furthermore, the enhancement of PTEN neddylation may result from the abnormal upregulation of XIAP and increased interaction between XIAP and PTEN.

PTEN neddylation enhances AP-1/JUND stability to promote Palbociclib resistance

To examine the role of PTEN neddylation on CDK4/6i resistance, we performed RNA-seq in early adaptative Palbociclib resistant breast cancer cells (Figure 3A) and PTEN neddylation mutated cells [28] (2KR, K197 and K402 sites mutated to R) (Figure 3B). Consistent with earlier studies [9-11], the results indicated that PI3K/Akt signaling pathway was closely associated with CDK4/6i resistance and PTEN neddylation (Figure S2A, S2C, 3A and 3B). However, it has reported that PI3K inhibitors show promise in delaying CDK4/6i resistance onset, but they fail to rescue cells from established resistance by reversing acquired insensitivity [10, 12]. With great interest, GSEA analysis indicated that MAPK signaling pathway obviously was also enriched (Figure 3C and 3D). Similar data was shown in the related dataset

(GSE222367 [31]) (Figure S2A). Of note, resistance to Palbociclib led to an upregulation of the AP-1 signaling pathway, including FOSB, FOSL, c-FOS, c-JUN, JUND and JUNB (Figure 3E and S2B). Conversely, PTEN neddylation mutation decreased the expression of these genes (Figure 3F). These results strongly suggest amplified AP-1 signaling pathway is an underlying mechanism of resistance to Palbociclib, and PTEN neddylation is involved in regulating AP-1 activity.

Therefore, we detected comparable elevated protein levels of Rb phosphorylation in acquired Palbociclib resistant breast cancer cells. Notably, there is a markable increase of JUND at the protein level (Figure 3G). Meanwhile, phosphorylation of JUND was also upregulated which indicated the activition of AP-1 (Figure 3H). Moreover, assessment of protein levels in the nuclear and cytoplasmic fractions showed a clear enrichment of nuclear JUND and phosphorylated JUND in acquired Palbociclib-resistant breast cancer cells (Figure 3I). Similar results were also found in acquired Palbociclib resistance primary breast cancer cells isolated from MMTV-*PyMT* mice and early adaptative Palbociclib resistance MCF-7 cells, not in T98G cells (Figure 3J and 3K). Our previous study has found that neddylation occurred at the final aminal acid of PTEN (K402) [28]. PTEN-Nedd8 is a fusion protein created by linking Nedd8 to the C-terminus of PTEN to mimic neddylated PTEN.

For comparison, a nuclear localization sequence (NLS) was fused to the N-terminus of PTEN (NLS-PTEN) [28,32,33]. We also observed an increase expression level of JUND and phosphorylated JUND in shPTEN+PTEN-Nedd8 stable MCF-7 cells, but

the opposite effect in shPTEN+PTEN-NLS stable cells (Figure 3L). JUND was also highly expressed and positively associated with PTEN neddylation in patients with HR+/HER2- breast cancer (Figure S2D-S2G). Collectivly, the results show that neddylation of PTEN enhances the protein expression and phosphorylation of JUND.

PTEN neddylation decreases JUND ubiquitination

Next, we intended to explore the mechanism by which PTEN neddylation promotes JUND protein expression, IP analysis indicated that compared with NLS-PTEN, PTEN-Nedd8 showed a higher affinity for JUND (Figure 4A). Then, we further investigated JUND ubiquitination and observed that PTEN-Nedd8 reduced the levels of ubiquitinated JUND (Figure 4B). In acquired Palbociclib-resistant breast cancer cells, the levels of ubiquitinated JUND were much lower than in Palbociclib-sensitive breast cancer cells (Figure 4C). To date, no specific ubiquitin ligase for JUND has been reported. UbiBrowser 2.0 (http://ubibrowser.ncpsb.org/) was employed to predict Ub E3 ligases interacting with JUND with high confidence [34,35]. Among the interactive protein candidates, ITCH (also known as AIP4) was predicted to be the E3 of JUND with the highest affinity (Figure S3A). ITCH overexpression induced a marked increase in JUND ubiquitination (Figure S3B). Further interaction experiments show that PTEN neddylation reduced the interaction between JUND and ITCH, leading to a decrease in the phosphorylation JUND (Figure 4D and Figure 4E).

Additionally, in acquired Palbociclib-resistant breast cancer cells, JUND decreased the interaction with ITCH (Figure 4F). Then, the interactions among ITCH ， JUND

and PTEN proteins were simulated using the AlphaFold2.0. Subsequently, the results showed that although PTEN interacted with JUND, it did not affect the binding of JUND to its ubiquitination E3-ITCH. However, when PTEN is covalently modified by nedd8, it occupid the binding site of ITCH and JUND, thereby interfering with their interaction and the transfer of ubiquitin. To further explore the role of PTEN neddylation on JUND, CUT & Tag analysis was performed in PTEN neddylation mutated cells. A total of 6306 unique genes were enriched in several KEGG pathways, including the PI3K/Akt signaling pathway, MAPK signaling pathway, and Ras signaling pathway (Figure 4H). CUT & Tag qPCR analysis demonstrated that in the absence of PTEN neddylation, JUND exhibited reduced enrichment at the promoters of downstream genes associated with inflammation and immune response, including CFS2, IL-17, IL-6, MMP13 and IL-1β (Figure 4I). Hence, we conclude that neddylation of PTEN enhances the stability of JUND by modulating its ubiquitination, leading to the activation of the AP-1 signaling pathway in Palbociclib-resistant breast cancer.

Identification of Echinacoside as a PTEN neddylation inhibitor.

Considering that PTEN neddylation influenced the responsiveness to Palbociclib therapy in breast cancer, we aimed to explore the possibility of disrupting the interplay between PTEN and XIAP, with the hypothesis that this strategy could potentially mitigate PTEN neddylation and thereby increase sensitivity to Palbociclib, particularly in overcoming resistance. Firstly, we sought to search the pivotal amino acid residues by examining the interacting interfaces between XIAP and PTEN.

Consistent with previous study [28, 36], XIAP was co-immunoprecipitated with PTEN *in vivo* (Figure S4A). The truncations containing BIR2 domain of XIAP and the C2 domain of PTEN interacted with one another (Figure S4B-S4D). Based on molecular docking method and *in vitro* pull-down assay, we found that Y154 and N234 sites at XIAP, as well as S207 and R335 sites at PTEN were indicated to be key binding sites on the interaction surface (Figure 5A and 5B).

On the basis of the binding determinants of the XIAP-PTEN interface, structure-based virtual screening was performed to find potential XIAP-PTEN PPI (protein and protein interaction) inhibitors (Figure 5C). Ultimately, we selected five compounds, guided by the top-ranking binding models and scores in the Enamine libraries containing protein-protein interacting compound collection and the Bioactive Compound Library Plus in *MedChemExpress* LLC (Figure S4E). No PPI inhibitors affected the protein and mRNA level of PTEN (Figure S4F and S4G). Among the five compounds, we noticed that Echinacoside (ECH), a natural phenylethanoid glycoside (the chemical formula was shown in Figure 4D), markedly interrupted the interaction between XIAP and PTEN (Figure S4H). ECH is one of the main phenylethanol glycosides isolated and purified from cistanche tubulosa, which has been used as traditional Chinese herbal medicine with anti-senility and antifatigue effects [37, 38]. ECH is the compound with the highest molecular docking score, and it is the only compound among the five that forms hydrogen bond interactions with the two critical amino acid sites, S207 and R335, of PTEN that interact with XIAP. (Figure 5E). Subsequently, we employed Surface Plasmon Resonance (SPR) analysis to evaluate

the interaction between ECH and PTEN. Dose-dependent binding profiles were successfully obtained. As illustrated in Figure 4F, ECH showed the highest binding affinity with PTEN. Further co-immunoprecipitation assays demonstrated that ECH effectively disrupted the interaction between the truncated XIAP and PTEN (Figure 5G). Pull-down assay revealed a clear dose-dependent decrease of the XIAP-PTEN C2 interaction following treatment with ECH (Figure 5H). Moreover, ECH did not affect the dimerization of PTEN (Figure 5I and 5J). Next, we aimed to detect whether inhibition of XIAP-PTEN PPI by ECH would affect PTEN neddylation. Neddylation assays revealed that ECH inhibited PTEN neddylation *in vivo*, but not PTEN ubiquitination (Figure 5K and S4I). *In vitro* neddylation assay indicated that ECH interfered XIAP mediated PTEN neddylation (Figure 5L). Further analysis revealed that ECH eliminated XIAP-PTEN interaction and PTEN neddylation in Palbociclib resistance breast cancer mice tissues (Figure 5M and 5N). Taken together, we identified Echinacoside (ECH), a natural phenylethanoid glycoside, as a potent PTEN neddylation inhibitor through structure simulation and biochemical analyses. The obtained results revealed that ECH eliminates PTEN neddylation by inhibiting the interplay between XIAP and PTEN in Palbociclib resistance breast cancer.

ECH is dependent on PTEN neddylation to suppress tumorigenesis.

Next, we intended to explore the role of ECH in tumorigenesis. ECH exhibited a significant tumor-suppressive effect, manifested in a dose-dependent manner, on cellular proliferation, colony formation, and cell migration across various tumor cell lines (Figure S5A-S5D). Then, we measured the drug toxicity of ECH in CD-1 mice.

The body weight showed no obvious difference between mice injected with ECH and the control (Figure S6A and S6B). No alterations in blood cell count or composition were observed after ECH treatment (Figure S6C). Moreover, analysis of serum ALT levels demonstrated no substantial difference between the ECH-treated groups and the control, suggesting the absence of obvious liver injury (Figure S6D). Additionally, body weight and histopathology of vital organs revealed no signs of toxicity or damage in both ECH-treated group and the vehicle control group (Figure S6E-S6G). Therefore, we speculated that ECH might demonstrate a favorable therapeutic profile with substantial anti-tumor efficacy and minimal adverse effects in breast cancer.

We then explored the requirement of PTEN neddylation for ECH-mediated anti-tumor effects. Deletion of PTEN notably weakened the inhibitory effects of ECH on cell proliferation (Figure 6A and 6B) and tumor invasion (Figure 6C). Moreover, Palbociclib showed increased the inhibitory effects on cell proliferation (Figure 6D and 6E) and increased the cell death (Figure 6F) in shPTEN+PTEN 2KR cell lines. However, the observation that ECH suppresses cell proliferation and elevates cell apoptosis was eliminated when PTEN was unable to be neddyated (Figure 6G and Figure 6H). Additionally, ECH was no longer decreased the protein level of JUND and p-JUND in shPTEN+PTEN 2KR cells (Figure 6I). As demonstrated in Figure 6J, upon exposure to ECH, the AP-1 related signaling pathways, including MAPK, VEGF, and JAK-STAT3, exhibited a notable decrease in shPTEN+PTEN-2KR mutation breast cancer cells. Due to MAPK, VEGF, and JAK-STAT3 signaling pathways are intricately connected to the tumor immune microenvironment, we

finally performed immunoassay arrays in shPTEN+PTEN-WT and 2KR breast cancer cells with ECH treatment or not. The data demonstrated a reduction in the levels of multiple cytokines and chemokines, including G-CSF, GM-CSF, IFN-γ, IL-1RA, IL-1β, IL-8, CCL2/4, IL-17 and VEGF, specifically in shPTEN+PTEN-WT cells following ECH administration; however, there were no alterations observed in the shPTEN+PTEN-2KR cells subsequent to ECH exposure (Figure 6K and 6L). Similar results of G-CSF, IL-1β, IL-17A were also approved by ELISA assay (Figure 6M). Therefore, the above evidences suggested that ECH exhibited oncogenic effects, at least to some extent, by interfering with PTEN neddylation. The above results also indicated that ECH exerts its regulation on the inflammatory immune factor composition within the tumor microenvironment through PTEN neddylation modification.

Combination ECH enhances the sensitivity of Palbociclib in HR+/HER2-breast cancer.

Considering excessive activation of PTEN neddylation is prone to foster Palbociclib resistance, we aimed to explore whether ECH might enhance sensitivity to Palbociclib resistance in breast cancer. Therefore, we next investigated the anti-tumor efficacy of ECH in Palbociclib resistance mouse models. After acquiring resistance to Palbociclib through prolonged the Palbociclib exposure in MMTV-*PyMT* mice, ECH was injected to observe the subsequent alterations of tumor dynamics (Figure 7A). As expected, the tumor weight and volume were both markedly declined in the Palbociclib resistance MMTV-*PyMT* mice following the treatment of ECH (Figure 7B-7D).

Primary breast cancer cells derived from the Palbociclib-resistant MMTV-*PyMT* mice displayed significantly reduced proliferation upon exposure to ECH treatment (Figure S7A and S7B). Similar results were also obtained from the tumor organoids of Palbociclib-resistant MMTV-*PyMT* mice (Figure S7C-S7E). The data from immunoassay arrays revealed that when PTEN is unable to undergo neddylation, there was an obvious reduction of GM-CSF and G-CSF (Figure 6K). It has been known that G-CSF functions as a mobilizing agent for neutrophils, while GM-CSF influences the development and functionality of both neutrophils and macrophages [39-41]. Then, flow cytometry was employed to isolate neutrophils and macrophages, where we observed a significant decrease in both macrophages and neutrophils in Palbociclib resistance MMTV-*PyMT* mice after ECH treatment (Figure 7E). Consequently, our findings suggest that ECH might reprogramme the tumor microenvironment by targeting PTEN neddylation, thereby sensitizing against Palbociclib resistance.

We next investigated the decline in protein expression levels of JUND and p-JUND, along with the suppression of the PI3K/Akt signaling pathway, which was observed both in early adaptative and acquired Palbociclib-resistant breast cancer cells (Figure 7F and Figure 7G) after ECH treatment. Similar results were also found in Palbociclib-resistant breast caner tissues of MMTV-*PyMT* mice (Figure S7F and S7G). Furthermore, there was a decrease in the ubiquitination of JUND within acquired Palbociclib-resistant breast cancer cells, which showed a notable increase upon exposure to ECH (Figure 7H). Multiplex immunohistochemical and immunohistochemical analyses disclosed an elevated level of PTEN neddylation and

the protein level of XIAP in breast cancer tissues from MMTV-*PyMT* mice that are Palbociclib-resistant, while treatment with ECH resulted in a notable decrease (Figure S7F-S7I). In addition, neddylation E1-UBA3, E2-Ubc12 and Nedd8 showed no obvious changes (Figure S7F and S7G). Finally, we intended to investigate the efficacy of combination of ECH with Palbociclib. The results showed significantly decreased cell proliferation compared with monotherapy (Figure 7I). We then intended to confirm the efficacy of combination therapy using tumor organoid models derived from human HR+/HER2- breast cancer patients (Figure S1A). Both ECH and Palbociclib monotherapies showed tumor growth suppression effects on tumor organoid models. Notably, the combination treatment exhibited an even better anti-tumor growth efficacy compared with the monotherapies (Figure 7J). Immunofluorescence staining revealed a significant reduction in PTEN neddylation modification following ECH treatment (Figure 7K). Meanwhile, in T98G cells that exhibit resistance to Palbociclib, the co-administration of ECH led to a notable increase in cellular sensitivity to Palbociclib, thereby suppressing tumor cell proliferation (Figure S8A and S8B). Taken together, these findings collectively illustrate that ECH serves as an effective sensitizing agent for Palbociclib in HR+/HER2- breast cancer, with the combined therapy showing a better anti-tumor activity.

DISCUSSION

Despite the remarkable clinical activity of CDK4/6 inhibitors, intrinsic and acquired resistance to these drugs is widespread and poorly understood. We report herein

PTEN neddylation modification as a mechanism of resistance to treatment with Palbociclib. We observed an increase in PTEN neddylation modification in HR+/HER2- breast cancer patients resistant to Palbociclib. Similar findings were also observed in both Palbociclib-resistant breast cancer cells and spontaneous breast cancer MMTV-*PyMT* mice (Figure 1). Palbociclib resistance led to upregulated expression of PTEN neddylation E3 ligase XIAP, which is consistent with previous study suggesting that compensatory CDK2 activation upon resistance could lead to increased XIAP mRNA levels [42, 43]. This dynamic resulted in enhanced binding to PTEN, thus contributing to the augmented PTEN neddylation observed after Palbociclib resistance (Figure 2).

We have proved that neddylated PTEN acts as a tumor-promoting protein rather than tumor-suppressing protein [28]. Regarding the mechanism of the Palbociclib resistance role of PTEN modified by nedd8, we showed that neddylation promoted the activity of PI3K/Akt signaling pathway. *PIK3CA* mutations occur in approximately 40% of HR-positive breast cancers, and activation of the PI3K/Akt signaling pathway is prominent as cancers become resistant to CDK4/6 inhibitors. While PI3K inhibitors hold promise in mitigating the onset of CDK4/6 inhibitor resistance, their efficacy in rescuing cells from established resistance falls short, as they are unable to reverse the acquired insensitivity [12, 44-47]. Our study demonstrates that, in addition to the PI3K/Akt signaling pathway, the MAPK/AP-1 signaling pathway is closely associated with resistance against Palbociclib. To understand how PTEN neddylation promotes resistance, we identified that neddylated

PTEN interacted with JUND. JUND is a component protein of the activating protein-1 (AP-1) transcription factor and is considered as a classical proto-oncogene. Dysfunctional AP-1 transcriptional activity is associated with tumor growth, invasion, migration and drug resistance [48-50]. As of yet, it has known that CDK4/6 inhibition reprograms the breast cancer enhancer landscape by stimulating AP-1 transcriptional activity, but the role of AP-1 in regulating resistance to CDK4/6 inhibitors remains unclear [51]. Here, we noticed that PTEN neddylation led to an obviously enhancement in JUND protein stability, rather than c-JUN, JUNB or FOS in Palbociclib resistance breast cancer cells and mouse models (Figure 3). So far, the protein stability regulation of JUND have remained elusive. We identified that ITCH as a polyubiquitination E3 ligase for JUND. Neddylated PTEN interacted with JUND to decrease the ubiquitination of JUND which was catalyzed by ITCH, thereby preventing the degradation of JUND. Through structural simulation, we observed that the protein structure of the PTEN protein might be changed by neddylation modification, affecting the binding of ITCH and JUND.

This mechanism resulted in enhanced JUND protein stability and increased JUND phosphorylation. Consequently, upon the transcriptional activation of AP-1, its downstream target genes such as IL-1, GM-CSF, TNFα are elevated (Figure 4). These results propose a novel aspect of PTEN neddylation to drive AP-1 activity in the resistance to Palbociclib therapy.

We next employed a specific small molecule inhibitor, Echinacoside (ECH), to interfere with the dynamic interplay between XIAP and PTEN, ultimately suppressing

the neddylation of PTEN (Figure 5). ECH, a key efficacious constituent found in *Echinacea*, is also abundantly present in various other natural plant sources, including the roots of *Scrophulariae*, *Rehmanniae*, and *Cistanches Herba*, among others [38]. It has been reported that ECH inhibits tumor metastasis *via* suppressing the PI3K/AKT signaling pathway, but the mechanism remains unclear [52-54]. Our findings indicated that ECH exhibits promising anti-tumor efficacy and drug safety. Small molecules targeting neddylation activating enzymes (E1), such as MLN4924 (trade name Pevonedistat) and TAS4464, have shown promise in clinical trials for cancer treatment [25, 55]. DI-404, DI-591, NAcM-HIT, NAcM-OPT, and WS-383 are competitive neddylation conjugating enzymes (E2) inhibitors that target UBE2M-DCN1 interaction [56-58]. HA-9104 is a targeted inhibitor of another E2-UBE2F [59]. However, given the limited number of neddylation E1 and E2, unbiased inhibition of the whole neddylation within cells might inadvertently harm normal cellular processes. Therefore, we believe targeting key neddylation substrates involved in the tumor process, would offer greater specificity, reduced drug side effects, and potentially more potent anti-tumor effects. For the first time, our study demonstrates that ECH is a selective inhibitor targeting neddylation substrates for anti-cancer therapy. It is worth noting that the anti-tumor activity of ECH depends on the regulation of PTEN neddylation modification. (Figure 6).

More importantly, ECH obviously elevates the sensitivity of Palbociclib, and ECH in combination with Palbociclib would more effectively reduce the tumor growth (Figure 7). Although the resistance mechanisms associated with CDK4/6 inhibitors in

breast cancer have been documented, but not fully elucidated. Targeted therapies basing these mechanisms have not effectively overcome resistance in breast cancer. For instance, of particular importance to mention is that the concurrent use of PI3K inhibitors like alpelisib or buparlisib alongside CDK4/6 inhibitors is clinically discouraged, primarily due to well-documented safety considerations [10,12]. Nonetheless, given PTEN plays pivotal role as a suppressor in the PI3K/Akt signaling pathway, we contend that restoring PTEN tumor-suppressive activity holds promise for more effectively inhibiting the PI3K/Akt signaling pathway. Additionaly, the tumour microenvironment (TME) has been well-established to mediate drug resistance. The impact of drug resistance on the TME of malignant tumors can be categorized into regulation of tumor-secreted cytokines [60, 61]. Targeting CDK4/6 has shown promise in augmenting the efficacy of immune checkpoint inhibitors, but a deeper understanding of its functional and mechanistic implications is lacking [62]. In this study, we found that neddylated PTEN upregulated the levels of multiple cytokines and chemokines, which might modulate the contents of TME to induce Palbociclib resistance. Ultimately, our findings unlock a promising therapeutic strategy by focusing on neddylation to effectively restorate PTEN tumor suppressor activity, thereby enhancing the efficacy of Palbociclib (Figure 7L). It highlights a deeper understanding of CDK4/6i resistance mechanisms and the development of advanced combination therapies in optimizing breast cancer treatment outcomes.

ACKNOWLEDGEMENTS

This study was supported by National Outstanding Youth Science Fund Project of National Natural Science Foundation of China (82122052), Outstanding Young Talents Program in Chinese Institutes for Medical Research, Beijing (CX23YQA03).

AUTHOR CONTRIBUTION

Conceptualization, P.X; Methodology, F.L., W.X.L., Y.X.S., S.H.L. and X.K.J.; Formal Analysis, F.L., W.X.L.; Investigation, P.X. and F.L.; Resources, S.Y.S., Y.W.T. and Z.Z.; Writing - Original Draft, P.X.; Funding Acquisition, P.X.

DECLARATION OF INTERESTS

The authors declare that there is no competing financial, commercial, or professional interest that could influence the performance, interpretation, or reporting of the research presented in this manuscript. All authors have read and approved this Declaration of Interests, confirming that it accurately reflects their current situation. The authors declare no competing interest.

METHODS

Resource Availability

Lead contact

Further information and requests for resources and reagents should be directed to and will be fulfilled by the lead contact, Ping Xie (xiep@ccmu.edu.cn).

Materials availability

This study did not generate new reagents.

Data and code availability

RNA-seq data have been deposited at SRA (PRJNA1143082 and PRJNA1144658) and are publicly available as of the date of publication. All other data are included in the main and supplemental materials.

Experimental model and subject details

Cell lines

All mammalian cells were cultured following ATCC recommended protocols and in medium supplemented with 10% fetal bovine serum (FBS, VivaCell BIOSCIENCES C04001-500) and 1% Penicillin-Streptomycin (Gene-Protien Link P08X14). MCF-7, HEK-293T, HCT116, A549, MDA-MB-231, MCF-7 shPTEN, MCF-7 shPTEN+PTEN-Nedd8, MCF-7 shPTEN+PTEN-NLS, MCF-7 shPTEN+PTEN-WT and MCF-7 shPTEN+PTEN-2KR cells were cultured in Dulbecco's modified Eagle's medium (DMEM) with high glucose (Thermo Fisher Scientific). T47D and T98G

cells were cultured in RPMI-1640 medium (Thermo Fisher Scientific C11875500BT). MCF-7 ADR was purchased from Sunncell Biosciences. MCF-7 DDP was purchased from Shanghai Mei Xuan Biological Technology Co., Ltd. MCF-7 PTX was purchased from BLUEFBIO (Shanghai, China).

Mice

The MMTV-*PyMT* mice (*PyMT*/WT mice, C57BL/6J background) and BALB/c nude mice (6-week old, 18.0±2.0 g) were purchased from Cyagen Biosciences. CD-1(ICR) mice were purchased from Beijing Vital River Laboratory Animal Technology Co., Ltd.

Patient inclusion and sample collection

The clinical samples were approved by the department of breast and thyroid surgery at the Second People's Hospital of Shenzhen. Informed consent was obtained from all subjects or their relatives.

Antibodies and chemicals

The following antibodies were used: Phospho-Rb (Ser807/811) (#8516), Rb (#9309), Cyclin D1 (#2922), PTEN (#9188), Ub (#20326), Akt (#9272), Phospho-Akt (Ser473) (#9271), Phospho-Akt (Thr308) (#13038), Phospho-JUND (Ser100) (#9164), CUL1(#4995), XIAP(#2042), Nedd8 (#2754), c-JUN (#9165T), JUNB (#3753T), c-FOS (#2250T) and FOSB (#2251T) antibodies were purchased from Cell Signaling Technology. Cyclin E (#sc-377100) antibody was purchased from Santa Cruz Biotechnology. GAPDH (#60004-1-Ig), UBA3 (#68067-1-Ig), Ubc12 (#CL488-67482), and GST (#HRP-66001) antibodies were purchased from

Proteintech. Flag (#M185-3L), Myc (#M047-3) and HA (#M132-3) antibodies were purchased from MBL. JUND (#A5433) and FOSL1 (#A5372) antibodies were purchased from ABclonal. The following chemicals were used: Palbociclib (HY-50767), Pevonedistat (HY-70062), Echinacoside (HY-N0020), Maltotetraose (HY-N2464), MG132 (HY-13259), Cisplatin (Y-17394), Paclitaxel (HY-B0015), Doxorubicin hydrochloride (HY-15142), Z21911837, Z45457765 and Z1549417413 were purchased from *Med Chem Express*.

Drug-resistant cell lines

Palbociclib-resistant cell line was generated by culturing each of the MCF-7 cell pools in complete medium supplemented with increasing concentrations of Palbociclib, 1.2 mmol/L, 2.4 mmol/L, 3.6 mmol/L, and 4.8 mmol/L, in a stepwise manner over a 6- to 7- month period.

Method details

RNA-seq Analysis

Trizol was utilized in compliance with the manufacturer's instructions to extract total RNA from MCF-7 cells treated by Palbociclib. After that, RNA was digested for reverse transcription, and rRNA was degraded. A complementary DNA library was prepared, and sequencing was performed according to the Illumina standard protocol by Novogene Technology Co., Ltd. (Beijing, China). The Kyoto Encyclopedia of Genes and Genomes (KEGG) was used for pathway analysis.

Immunoprecipitation and immunoblotting

For immunoprecipitation assays, cells were lysed in EBC lysis buffer (0.5% NP-40,

50 mM Tris, pH 7.6, 120mM NaCl, 1mM EDTA, 1mM Na_3VO_4, 50mM NaF and 1mM β-mercaptoethanol) supplemented with protease inhibitor cocktail (Roche, 11836170001). Immunoprecipitations were performed using the indicated primary antibody and Dynabeads™ protein G beads (10004D) at 4°C. The immunoprecipitants were washed at least three times in EBC lysis buffer before being resolved by SDS-PAGE and immunoblotted with indicated antibodies.

***In vivo* modification assays**

Cells were solubilized in modified lysis buffer (50 mM Tris, pH 7.4, 150mM NaCl, 10% glycerol, 1mM EDTA, 1mM EGTA, 1% SDS, 1 mM Na_3VO4, 1mM DTT and 10mM NaF) supplemented with a protease inhibitor cocktail. The cell lysate was incubated at 4 °C for 10min. The lysate was then diluted 10 times with modified lysis buffer without SDS and incubated with the indicated antibody for 3h at 4°C before adding Dynabeads™ protein G beads (10004D). Then the lysate was rotated gently for 8 h at 4°C. The immunoprecipitants were washed at least three times in wash buffer (50mM Tris, pH7.4, 150mM NaCl, 10% glycerol, 1mM EDTA, 1mM EGTA, 0.1% SDS, 1mM DTT and 10mM NaF). Proteins were analyzed by western blotting with indicated antibodies.

***In vitro* modification assays**

In vitro modification assays GST-PTEN and GST-Ubc12 were expressed in Escherichia coli BL21 (DE3). For the Neddylation assay, 0.5μg of GST-PTEN, 0.5μg of GST-Ubc12 were incubated with 2μg of Nedd8, 10ng of E1 (APPBP1 UBA3) and 0.5μg of E3 (His-XIAP) in a total reaction volume of 30μL Nedd8 conjugation Rxn

Buffer Kit (Boston Biochem, SK-20). Nedd8 (UL-812), Nedd8 E1 (APPBP1/UBA3) (E-313), His-XIAP were purchased from Boston Biochem. Samples were incubated at 37°C for 30min, and reactions were terminated with SDS-PAGE loading buffer before western blotting.

GST Pull down

Bacterial-expressed GST and GST–PTEN bound to BeyoGold™ GST-tag Purification Resin (P2250) was incubated with Myc-XIAP or their truncates expressed in HEK293T cells for 2 h at 4 °C. Then the beads were washed with GST binding buffer (100 mM NaCl, 10 mM Tris, 50 mM NaF, 2 mM EDTA, 0.5 mM Na_3VO_4 and 1% NP40) three times and proteins were eluted, followed by western blotting.

Real-time PCR

For real-time quantitative PCR (RT-qPCR) assay, 1 μg of total RNA was reverse-transcribed into cDNA using ReverTra Ace® qPCR RT Master Mix （FSQ-201， TOYOBO). An equal amount of cDNA from different samples was mixed with Power SYBR green PCR master mix (CAT#QPK-201， TOYOBO). Gene-specific mRNA level for each experimental condition was determined using the ΔΔCT method. RT-qPCR results were presented as fold change of gene expression in the test samples compared to the control.

PTEN: forward, 5’-TGGATTCGACTTAGACTTGACCT-3’; reverse, 5’-TGGATTCGACTTAGACTTGACCT-3’;

GAPDH: forward, 5’-GGAGCGAGATCCCTCCAAAAT-3’; reverse, 5’-GGCTGTTGTCATACTTCTCATGG-3’

Molecular docking and virtual screening

The cryo-EM structure of human PTEN (PDB ID5R) was used to perform structure-based virtual screening via a workflow application of Glide in Maestro (Schrödinger Maestro 11.4). The Protein-Protein Interaction Library and the MCE Bioactive Compound Library Plus were selected as screening databases. The LigPrep module of Maestro was used to generate the three-dimensional (3D) conformations of the compounds. At the very beginning, the compounds were screened using the high-throughput virtual screening module and the top-ranked 20% candidates were selected on the basis of the Glide G-score. Then these candidates were redocked using the standard precision and extra precision mode in turn. Finally, 200 compounds with shape rationality and structural diversity were picked for assay.

Surface Plasmon Resonance binding assays

Surface plasmon resonance experiments were performed on a BIACORE 3000 biosensor system (GE Healthcare) according to the manufacturer's instructions at 25 °C. PTEN protein was immobilized onto a CM5 chip (GE Healthcare), which was activated using a 1:1 mixture of 1-ethyl-3-(3-dimethyllaminopropyl) carbodiimide (EDC) and N-hydroxysuccinimide (NHS) at a flow rate of 10 μL/min. ECH was diluted in PBS, and then injected over the PTEN surface at a rate of 30μL/min flow rate. The duration of protein binding time was set to 180 s, after which the running buffer was injected at the same rate for 300 s. The binding kinetics was processed and calculated by BIAevaluation software.

Cell proliferation assay

Cells were plated on 96-well plates (2000 cells per well). After adding Cell Counting Kit-8 (Dojindo, CK04) to the wells for 1 h, cell numbers were measured at 450 nm. Each cell line was set up in 3 replicate wells, and the experiment was repeated three times.

Cell migration assay

Cell migration assay was performed using Cell culture inserts for 24-well plates with 8.0 μm pores filter, and the filter was pre-coated with 20 μg/ml Fibronectin. A cell suspension in serum-free culture medium (5×10^4 cells per well) was added to the inserts, and each insert was placed in the lower chamber containing 10% FBS culture medium. After 24 h, cells were fixed using 4% paraformaldehyde for 20 min and stained using 0.1% crystal violet for 15 min. Cells in upper chamber were carefully removed, and cells migrated through the filter were assessed by photography.

Colony formation assay

Cells were seeded into 6-well tissue culture plate with 2000 cells per well. Plates were incubated at 37 °C and 5% CO_2 and colonies were scored 14 days after preparation. Each cell line was set up in 3 replicate wells, and the experiment was repeated three times.

Immunflorescence

Cells were fixed with 4% paraformaldehyde-PBS for 15 min. Following permeabilization and blocking, cells were incubated with primary antibodies overnight at 4°C. Secondary antibodies used were Alexa Fluor 488 or 568 (Invitrogen, 1:500 dilution). Samples were stained using DAPI (Beyotime C1002), and

immunofluorescence was detected using Leica confocal microscopy.

Tumor organoid culture

The breast cancer tissue was minced and digested with 5 ml of TrypLE (gibco 12605-010) digestion solution at 37 °C for 1 h. Using 5 mL medium terminate digestion and centrifugation (300 g for 5 min). Wash with 10 mL PBS and then filter with a cell strainer of 70 μm and centrifuge (300 g for 5 min). Pre-chilled pipette tips take 50 μL of pre-chilled organoid complete medium to resuspend the bottom cells and place them on ice, and 250 μL of Matrigel is added to the cell suspension. Remove the pre-warmed 96-well plate and aspirate 30 μL of each drop of cell suspension into the cell well plate with a pre-chilled pipette tip. Quickly invert the cell well plate, place it in a 37°C, 5% incubator and incubate for 15min until the matrix gel solidifies, and then add an appropriate volume of organoid complete medium after solidification.

CUT&Tag sequencing

CUT&Tag assay was performed using NovoNGS CUT&Tag 3.0 High-Sensitivity Kit (for Illumina, Novoprotein scientific Inc., Cat#N259-YH01-01A). Briefly, 1×10^5 cells were harvested freshly. Then 37% formaldehyde was gently added to cells and these samples were incubated at room temperature for 2 min. Cross-linking was stopped by addition of 1.25 M glycine and then the samples were washed with the wash buffer. The cells were enriched by ConA Beads and resuspended by 50 μL primary antibody buffer of anti-JUND antibody, and incubated overnight at 4 °C. Then discarded the primary antibody buffer and added 100 μL anti-rabbit IgG

antibody buffer for 1 h at a dilution of 1:100. Then the beads were washed for 3 times using antibody buffer and then incubated with protein A/G-Tn5 transposome for 1 h and washed for 3 times by ChiTaq buffer. Cells were resuspended in 50 μL Tagmentation buffer and incubated at 37 °C for 1 h. The incubation was stopped by adding 10 μL 10% SDS at 55 °C for 10 min. The DNA fragments were extracted by Tagment DNA extract beads and amplified using 5× AmpliMix. Then the DNA was re-extracted by DNA clean beads for sequencing.

CUT&Tag qPCR

The CUT&Tag qPCR experiments were conducted using Hyperactive Universal CUT&Tag Assay Kit from Vazyme (TD904), and experiments were conducted according to the instructions. The qPCR primers were as follows:

IL-1β promoter: forward, 5'- CAGAGTTCCCCAACTGGTACATC-3'; reverse, 5'-GGGAAGGCATTAGAAACAGTGTC-3';

IL-6 promoter: forward, 5'-TCTGCAAGATGCCACAAGGT-3'; reverse, 5'-TGAAGCCCACTTGGTTCAGG-3';

IL-17 promoter: forward, 5'-GCCTTTGTGATTGTTTCTTGCAG-3'; reverse, 5'-CCTTGCCCAAAGAAACCCTCTC-3';

CSF2 promoter: forward, 5'-TGTCGGTTCTTGGAAAGGTTCA-3'; reverse, 5'-TGTGGAATCTCCTGGCCCTTA;

MMP13 promoter: forward, 5'-CAACCATGGGGCTCAATCCT-3'; reverse, 5'-CTTACGTGGCGACTTTTTCTTTTC.

Flow cytometry Sorting

The types of the immune cell was identified by flow cytometry staining with PE -conjugated anti-F4/80 (BioLegend, 123109), BV421-conjugated anti-Ly6G (BioLegend, 127627), FITC-conjugated anti-CD8α (BioLegend, 100705) and APC-conjugated anti-CD4 (BioLegend, 100411) Samples were washed in FACS buffer and stained with the corresponding antibodies for surface marker analysis. Data were analyzed using FlowJo software.

Cohort and immunohistochemistry

The breast tissue microarrays were purchased from Shanghai Biochip Company (HBreD090Bc03) and Shanghai Zhuoli Biotech Company (ZL-Brcsur1801). HBreD090Bc03 were immunostained with Nedd8-PTEN K402 and JUND antibody. ZL-Brcsur1801 was immunostained with Nedd8-PTEN K402 antibody. Breast cancer tumors tissues were approved by the department of breast and thyroid Surgery at the Second People's Hospital of Shenzhen. All staining was assessed by a quantitative imaging method; the percentage of immunostaining and the staining intensity were recorded. An H-score was calculated using the following formula: H-score = Σ (PI × I) = (percentage of cells of weak intensity × 1) + (percentage of cells of moderate intensity × 2) + (percentage of cells of strong intensity × 3). PI indicates the percentage of positive cells versus all cells.

Multiplex immunohistochemical

Pheno 7-plex IHC kit (Pheno, PVB2002) was used according to manufacturer’s protocol. Slides were deparaffinised in xylene and rehydrated with 100%, 95%, 75% ethanol and double distilled water. Antigen was retrieved by citrate buffer and heated

to boil in microwave for approximately 20 min, sections were then blocked with bovine serum albumin at room temperature for 10 min. Primary antibodies were incubated at 37°C for 30 min, secondary antibody conjugated with horseradish peroxidase was incubated at room temperature for 10 min. Tyramide signal amplification was performed with 1:100 in antibody dilution buffer diluted fluorophores and incubated at room temperature for 10 min. Nuclei were stained with DAPI after primary antibodies were stained.

ELISA assay

The quantitation of IL-1β, IL-17A and G-CSF levels were performed using ELISA assay kit (Solarbio, SEKM-0002, SEKH-0026, and SEKH-0058) according to the manufacturer's instructions.

Immunoassay arrays

Concentrations of supernatants of MCF-7 shPTEN+PTEN WT/2KR cells cytokines were measured using the CBA (Cytometric Bead Array, RayBiotech FAH-STRM-1). Read samples on a flow cytometer and analyze using FCAP Array software (BD Biosciences).

Statistical analysis

All data were representative of no less than three independent experiments. All data were presented as means ± SD. Data were analyzed using SPSS 19.0 (IBM Corp., Armonk, NY, USA) and GraphPad Prism 5 (GraphPad Software, Inc., La Jolla, CA). The differences between groups were assessed by Student's t-test. The correlations were analyzed using Pearson correlation test. A value of $P<0.05$ was considered to be

statistically significant.

Ethics statement

All animals were handled in strict accordance to the "Guide for the Care and Use of Laboratory Animals" and the "Principles for the Utilization and Care of Vertebrate Animals", and all animal work was approved by Capital Medical University Ethics Committee.The clinical samples were approved by the department of breast and thyroid surgery at the Second People's Hospital of Shenzhen. Informed consent was obtained from all subjects or their relatives.

Supplemental information titles and legends

Supplementary material. Figures S1-S8.

REFERENCE

1. Nolan, E., Lindeman, G. J., Visvader, and J. E. (2023). Deciphering breast cancer: from biology to the clinic. Cell *186,* 1708–1728.

2. Harbeck, N., and Gnant, M. (2017). Breast cancer. Lancet *389*, 1134–1150.

3. Giuliano, M., Schettini, F., Rognoni, C., Milani, M., Jerusalem, G., Bachelot, T., De Laurentiis, M., Thomas, G., De Placido, P., Arpino, G., et al. (2019). Endocrine treatment versus chemotherapy in postmenopausal women with hormone receptor-positive, HER2-negative, metastatic breast cancer: a systematic review and network meta-analysis. Lancet Oncol *20*, 1360–1369.

4. Goel, S., Bergholz, J. S., and Zhao, J. J. (2022). Targeting CDK4 and CDK6 in cancer. Nat Rev Cancer *22*, 356–372.

5. Morrison, L., Loibl, S., and Turner, N. C. (2024). The CDK4/6 inhibitor revolution - a game-changing era for breast cancer treatment. Nat Rev Clin Oncol *21*, 89–105.

6. O'Sullivan, C. C., Clarke, R., Goetz, M. P., and Robertson, J. (2023). Cyclin-Dependent Kinase 4/6 Inhibitors for Treatment of Hormone Receptor-Positive, ERBB2-Negative Breast Cancer: A Review. JAMA Oncol *9*, 1273–1282.

7. Portman, N., Alexandrou, S., Carson, E., Wang, S., Lim, E., and Caldon, C. E. (2019). Overcoming CDK4/6 inhibitor resistance in ER-positive breast cancer. Endocr Relat Cancer *26*, R15–R30.

8. Lloyd, M. R., Spring, L. M., Bardia, A., and Wander, S. A. (2022). Mechanisms of Resistance to CDK4/6 Blockade in Advanced Hormone Receptor-positive, HER2-negative Breast Cancer and Emerging Therapeutic Opportunities. Clin Cancer Res *28*, 821–830.

9. Cai, Z., Wang, J., Li, Y., Shi, Q., Jin, L., Li, S., Zhu, M., Wang, Q., Wong, L. L., Yang, W., et al. (2023). Overexpressed Cyclin D1 and CDK4 proteins are responsible for the resistance to CDK4/6 inhibitor in breast cancer that can be reversed by PI3K/mTOR inhibitors. Sci China Life Sci 66, 94–109.

10. Herrera-Abreu, M. T., Palafox, M., Asghar, U., Rivas, M. A., Cutts, R. J., Garcia-Murillas, I., Pearson, A., Guzman, M., Rodriguez, O., Grueso, J., et al. (2016). Early Adaptation and Acquired Resistance to CDK4/6 Inhibition in Estrogen Receptor-Positive Breast Cancer. Cancer Res *76*, 2301–2313.

11. Wander, S. A., Cohen, O., Gong, X., Johnson, G. N., Buendia-Buendia, J. E., Lloyd, M. R., Kim, D., Luo, F., Mao, P., Helvie, K., et al. (2020). The Genomic Landscape of Intrinsic and Acquired Resistance to Cyclin-Dependent Kinase 4/6 Inhibitors in Patients with Hormone Receptor-Positive Metastatic Breast Cancer. Cancer Discov *10*, 1174–1193.

12. Clark, A. S., Makhlin, I., and DeMichele, A. (2021). Setting the Pick: Can PI3K Inhibitors Circumvent CDK4/6 Inhibitor Resistance? Clin Cancer Res *27*, 371–373.

13. Di Cristofano, A., and Pandolfi, P. P. (2000). The multiple roles of PTEN in tumor suppression. Cell *100*, 387–390.

14. Song, M. S., Salmena, L., and Pandolfi, P. P. (2012). The functions and regulation of the PTEN tumour suppressor. Nat Rev Mol Cell Biol *13*, 283–296.

15. Lee, Y. R., Chen, M., and Pandolfi, P. P. (2018). The functions and regulation of the PTEN tumour suppressor: new modes and prospects. Nat Rev Mol Cell Biol *19*, 547–562.

16. Papa, A., and Pandolfi, P. P. (2019). The PTEN-PI3K Axis in Cancer. Biomolecules *9*, 153.

17. Costa, C., Wang, Y., Ly, A., Hosono, Y., Murchie, E., Walmsley, C. S., Huynh, T., Healy, C., Peterson, R., Yanase, S., et al. (2020). PTEN Loss Mediates Clinical Cross-Resistance to CDK4/6 and PI3Kα Inhibitors in Breast Cancer. Cancer Discov *10*, 72–85.

18. Dosil, M. A., Mirantes, C., Eritja, N., Felip, I., Navaridas, R., Gatius, S., Santacana, M., Colàs, E., Moiola, C., Schoenenberger, J. A., et al. (2017). Palbociclib has antitumour effects on Pten-deficient endometrial neoplasias. J Pathol *242*, 152–164.

19. Lee, J. S., Yost, S. E., Li, S. M., Cui, Y., Frankel, P. H., Yuan, Y. C., Schmolze, D., Egelston, C. A., Guo, W., Murga, M., et al. (2022). Genomic Markers of CDK4/6 Inhibitor Resistance in Hormone Receptor Positive Metastatic Breast Cancer. Cancers *14*, 3159.

20. Lee, Y. R., Chen, M., Lee, J. D., Zhang, J., Lin, S. Y., Fu, T. M., Chen, H., Ishikawa, T., Chiang, S. Y., Katon, J., et al. (2019). Reactivation of PTEN tumor suppressor for cancer treatment through inhibition of a MYC-WWP1 inhibitory pathway. Science *364*, eaau0159.

21. Lin, Y. X., Wang, Y., Ding, J., Jiang, A., Wang, J., Yu, M., Blake, S., Liu, S., Bieberich, C. J., Farokhzad, O. C., et al. (2021). Reactivation of the tumor suppressor PTEN by mRNA nanoparticles enhances antitumor immunity in preclinical models. Sci Transl Med *13*, eaba9772.

22. Chaudagar, K., Hieromnimon, H. M., Kelley, A., Labadie, B., Shafran, J., Rameshbabu, S., Drovetsky, C., Bynoe, K., Solanki, A., Markiewicz, E., et al. (2023). Suppression of Tumor Cell Lactate-generating Signaling Pathways Eradicates Murine PTEN/p53-deficient Aggressive-variant Prostate Cancer via Macrophage Phagocytosis. Clin Cancer Res *29*, 4930–4940.

23. von Arnim A. G. (2001). A hitchhiker's guide to the proteasome. Sci STKE *2001*, pe2.

24. Enchev, R. I., Schulman, B. A., and Peter, M. (2015). Protein neddylation: beyond cullin-RING ligases. Nat Rev Mol Cell Biol *16*, 30–44.

25. Soucy, T. A., Smith, P. G., Milhollen, M. A., Berger, A. J., Gavin, J. M., Adhikari, S., Brownell, J. E., Burke, K. E., Cardin, D. P., Critchley, S., et al. (2009). An inhibitor of NEDD8-activating enzyme as a new approach to treat cancer. Nature *458,* 732–736.

26. Jiang, Y., and Jia, L. (2015). Neddylation Pathway as a Novel Anti-cancer Target: Mechanistic Investigation and Therapeutic Implication. Anticancer Agents Med Chem *15*, 1127–1133.

27. Zhang, S., Yu, Q., Li, Z., Zhao, Y., and Sun, Y. (2024). Protein neddylation and its role in health and diseases. Signal Transduct Target Ther *9*, 85.

28. Xie, P., Peng, Z., Chen, Y., Li, H., Du, M., Tan, Y., Zhang, X., Lu, Z., Cui, C. P., Liu, C. H., et al. (2021). Neddylation of PTEN regulates its nuclear import and promotes tumor development. Cell Res *31*, 291–311.

29. Du, M. G., Peng, Z. Q., Gai, W. B., Liu, F., Liu, W., Chen, Y. J., Li, H. C., Zhang, X., Liu, C. H., Zhang, L. Q., et al. (2021). The Absence of PTEN in Breast Cancer Is a Driver of MLN4924 Resistance. Front Cell Dev Biol *9*, 667435.

30. Guiley, K. Z., Stevenson, J. W., Lou, K., Barkovich, K. J., Kumarasamy, V., Wijeratne, T. U., Bunch, K. L., Tripathi, S., Knudsen, E. S., Witkiewicz, A. K., Shokat, et al. (2019). p27 allosterically activates cyclin-dependent kinase 4 and antagonizes palbociclib inhibition. Science, *366*, 6471.

31. Navarro-Yepes, J., Kettner, N. M., Rao, X., Bishop, C. S., Bui, T. N., Wingate, H. F., Singareeka Raghavendra, A., Wang, Y., Wang, J., Sahin, A. A., et al. (2023). Abemaciclib Is Effective in Palbociclib-Resistant Hormone Receptor-Positive Metastatic Breast Cancers. Cancer Res *83*, 3264–3283.

32. Liu, F., Wagner, S., Campbell, R. B., Nickerson, J. A., Schiffer, C. A., and Ross, A. H. (2005). PTEN enters the nucleus by diffusion. J Cell Biochem *96*, 221–234.

33. Planchon, S. M., Waite, K. A., and Eng, C. (2008). The nuclear affairs of PTEN. J Cell Sci *121*, 249–253.

34. Li, Y., Xie, P., Lu, L., Wang, J., Diao, L., Liu, Z., Guo, F., He, Y., Liu, Y., Huang, Q., et al. (2017). An integrated bioinformatics platform for investigating the human E3 ubiquitin ligase-substrate interaction network. Nat Commun *8*, 347.

35. Wang, X., Li, Y., He, M., Kong, X., Jiang, P., Liu, X., Diao, L., Zhang, X., Li, H., Ling, X., et al. (2022). UbiBrowser 2.0: a comprehensive resource for proteome-wide known and predicted ubiquitin ligase/deubiquitinase-substrate interactions in eukaryotic species. Nucleic Acids Res *50*, D719–D728.

36. Van Themsche, C., Leblanc, V., Parent, S., and Asselin, E. (2009). X-linked inhibitor of apoptosis protein (XIAP) regulates PTEN ubiquitination, content, and

compartmentalization. J Biol Chem *284*, 20462–20466.

37. Facino, R. M., Carini, M., Aldini, G., Saibene, L., Pietta, P., and Mauri, P. (1995). Echinacoside and caffeoyl conjugates protect collagen from free radical-induced degradation: a potential use of Echinacea extracts in the prevention of skin photodamage. Planta Med *61*, 510–514.

38. Wang, W., Jiang, S., Zhao, Y., and Zhu, G. (2023). Echinacoside: A promising active natural products and pharmacological agents. Pharmacol Res *197*, 106951.

39. Chen, B. D., Clark, C. R., and Chou, T. H. (1988). Granulocyte/macrophage colony-stimulating factor stimulates monocyte and tissue macrophage proliferation and enhances their responsiveness to macrophage colony-stimulating factor. Blood *71*, 997–1002.

40. Spiekermann, K., Roesler, J., Emmendoerffer, A., Elsner, J., and Welte, K. (1997). Functional features of neutrophils induced by G-CSF and GM-CSF treatment: differential effects and clinical implications. Leukemia *11*, 466–478.

41. Kolaczkowska, E., and Kubes, P. (2013). Neutrophil recruitment and function in health and inflammation. Nat Rev Immunol *13*, 159–175.

42.Dong, F., Guo, W., Zhang, L., Wu, S., Teraishi, F., Davis, J. J., and Fang, B. (2006). Downregulation of XIAP and induction of apoptosis by the synthetic cyclin-dependent kinase inhibitor GW8510 in non-small cell lung cancer cells. Cancer Biol Ther *5*, 165–170.

43. Chen, Q., Chen, K., Guo, G., Li, F., Chen, C., Wang, S., Nalepa, G., Huang, S., and Chen, J. L. (2014). A critical role of CDKN3 in Bcr-Abl-mediated tumorigenesis. PloS One *9*, e111611.

44. Burgoyne, A. M., Vann, K. R., Joshi, S., Morales, G. A., Vega, F. M., Singh, A., Pal, D., Merati, A. B., Kutateladze, T. G., and Durden, D. L. (2020). A triple action CDK4/6-PI3K-BET inhibitor with augmented cancer cell cytotoxicity. Cell Discov *6*, 49.

45. Agostinetto, E., Debien, V., Marta, G. N., Lambertini, M., Piccart-Gebhart, M., and de Azambuja, E. (2021). CDK4/6 and PI3K inhibitors: A new promise for patients with HER2-positive breast cancer. Eur J Clin Invest *51*, e13535.

46. Lawson, M., Cureton, N., Ros, S., Cheraghchi-Bashi, A., Urosevic, J., D'Arcy, S., Delpuech, O., DuPont, M., Fisher, D. I., Gangl, E. T., et.al (2023). The Next-Generation Oral Selective Estrogen Receptor Degrader Camizestrant (AZD9833) Suppresses ER+ Breast Cancer Growth and Overcomes Endocrine and CDK4/6 Inhibitor Resistance. Cancer Res *83*, 3989–4004.

47. Lee, C. L., Cremona, M., Farrelly, A., Workman, J. A., Kennedy, S., Aslam, R., Carr, A., Madden, S., O'Neill, B., Hennessy, B. T., et al (2023). Preclinical evaluation of the CDK4/6 inhibitor Palbociclib in combination with a PI3K or MEK inhibitor in colorectal cancer. Cancer Biol Ther *24*, 2223388.

48. Shaulian, E., and Karin, M. (2002). AP-1 as a regulator of cell life and death. Nat Cell Biol *4*, E131–E136.

49. Eferl, R., and Wagner, E. F. (2003). AP-1: a double-edged sword in tumorigenesis. Nat Rev Cancer *3*, 859–868.

50. Ruiz, E. J., Lan, L., Diefenbacher, M. E., Riising, E. M., Da Costa, C., Chakraborty, A., Hoeck, J. D., Spencer-Dene, B., Kelly, G., David, J. P., et.al (2021). JunD, not c-Jun, is the AP-1 transcription factor required for Ras-induced lung cancer. JCI Insight *6*, e124985.

51. Watt, A. C., Cejas, P., DeCristo, M. J., Metzger-Filho, O., Lam, E. Y. N., Qiu, X., BrinJones, H., Kesten, N., Coulson, R., Font-Tello, A., et.al (2021). CDK4/6 inhibition reprograms the breast cancer enhancer landscape by stimulating AP-1 transcriptional activity. Nat cancer *2*, 34–48.

52. Liu, J., Tang, N., Liu, N., Lei, P., and Wang, F. (2022). Echinacoside inhibits the proliferation, migration, invasion and angiogenesis of ovarian cancer cells through PI3K/AKT pathway. J Mol Histol *53,* 493–502.

53. Liang, H., Yin, G., Shi, G., Liu, Z., Liu, X., and Li, J. (2024). Echinacoside regulates PI3K/AKT/HIF-1α/VEGF cross signaling axis in proliferation and apoptosis of breast cancer. Anal Biochem *684*, 115360.

54. Wei, J., Zheng, Z., Hou, X., Jia, F., Yuan, Y., Yuan, F., He, F., Hu, L., and Zhao, L. (2024). Echinacoside inhibits colorectal cancer metastasis via modulating the gut microbiota and suppressing the PI3K/AKT signaling pathway. J Ethnopharmacol *318*, 116866.

55. Yamamoto, N., Shimizu, T., Yonemori, K., Kitano, S., Kondo, S., Iwasa, S., Koyama, T., Sudo, K., Sato, J., Tamura, K., et.al (2021). A first-in-human, phase 1 study of the NEDD8 activating enzyme E1 inhibitor TAS4464 in patients with advanced solid tumors. Invest New Drugs *39*, 1036–1046.

56. Zhou, H., Lu, J., Liu, L., Bernard, D., Yang, C. Y., Fernandez-Salas, E., Chinnaswamy, K., Layton, S., Stuckey, J., Yu, Q., et.al (2017). A potent small-molecule inhibitor of the DCN1-UBC12 interaction that selectively blocks cullin 3 neddylation. Nat Commun *8*, 1150.

57. Zhou, H., Zhou, W., Zhou, B., Liu, L., Chern, T. R., Chinnaswamy, K., Lu, J., Bernard, D., Yang, C. Y., Li, S., et.al (2018). High-Affinity Peptidomimetic Inhibitors of the DCN1-UBC12 Protein-Protein Interaction. J Med Chem *61*, 1934–1950.

58. Zheng, Y. C., Guo, Y. J., Wang, B., Wang, C., Mamun, M. A. A., Gao, Y., and Liu, H. M. (2021). Targeting neddylation E2s: a novel therapeutic strategy in cancer. J Hematol Oncol *14*, 57.

59. Xu, T., Ma, Q., Li, Y., Yu, Q., Pan, P., Zheng, Y., Li, Z., Xiong, X., Hou, T., Yu, B., et.al (2022). A small molecule inhibitor of the UBE2F-CRL5 axis induces apoptosis and radiosensitization in lung cancer. Signal Transduct Target Ther *7*, 354.

60. Vasan, N., Baselga, J., and Hyman, D. M. (2019). A view on drug resistance in cancer. Nature *575*, 299–309.

61. Zhang, Q. F., Li, J., Jiang, K., Wang, R., Ge, J. L., Yang, H., Liu, S. J., Jia, L. T., Wang, L., and Chen, B. L. (2020). CDK4/6 inhibition promotes immune infiltration in

ovarian cancer and synergizes with PD-1 blockade in a B cell-dependent manner. Theranostics *10*, 10619–10633.

62. Teh, J. L. F., and Aplin, A. E. (2019). Arrested Developments: CDK4/6 Inhibitor Resistance and Alterations in the Tumor Immune Microenvironment. Clin Cancer Res *25*, 921–927.

Figure 1

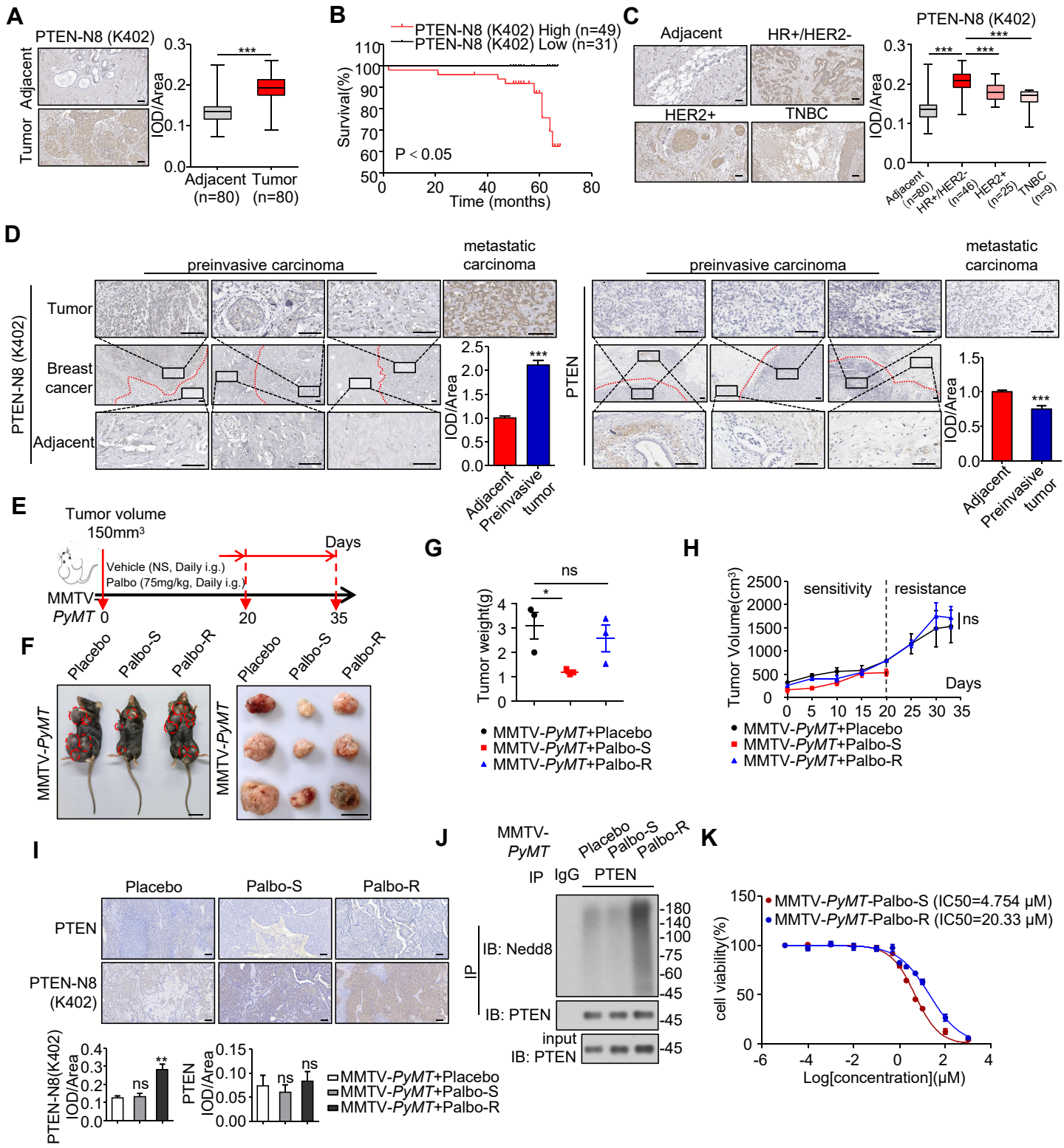
A
PTEN-N8 (K402)
Adjacent
Tumor
IOD/Area
Adjacent (n=80)
Tumor (n=80)
B
PTEN-N8 (K402) High (n=49)
PTEN-N8 (K402) Low (n=31)
Survival(%)
P < 0.05
Time (months)
C
Adjacent
HR+/HER2-
HER2+
TNBC
PTEN-N8 (K402)
IOD/Area
Adjacent (n=80)
HR+/HER2- (n=46)
HER2+ (n=25)
TNBC (n=9)
D
preinvasive carcinoma
metastatic carcinoma
PTEN-N8 (K402)
Tumor
Breast cancer
Adjacent
IOD/Area
Adjacent
Preinvasive tumor
PTEN
E
Tumor volume 150mm³
Days
Vehicle (NS, Daily i.g.)
Palbo (75mg/kg, Daily i.g.)
MMTV-PyMT
0
20
35
F
Placebo
Palbo-S
Palbo-R
MMTV-PyMT
G
Tumor weight(g)
MMTV-PyMT+Placebo
MMTV-PyMT+Palbo-S
MMTV-PyMT+Palbo-R
H
Tumor Volume(cm³)
sensitivity
resistance
ns
Days
MMTV-PyMT+Placebo
MMTV-PyMT+Palbo-S
MMTV-PyMT+Palbo-R
I
Placebo
Palbo-S
Palbo-R
PTEN
PTEN-N8 (K402)
PTEN-N8(K402) IOD/Area
PTEN IOD/Area
MMTV-PyMT+Placebo
MMTV-PyMT+Palbo-S
MMTV-PyMT+Palbo-R
J
MMTV-PyMT
Placebo
Palbo-S
Palbo-R
IP
IgG
PTEN
IB: Nedd8
IB: PTEN
input
IB: PTEN
K
MMTV-PyMT-Palbo-S (IC50=4.754 μM)
MMTV-PyMT-Palbo-R (IC50=20.33 μM)
cell viability(%)
Log[concentration](μM)

Figure 1 High PTEN neddylation levels associated with lack of response to CDK4/6i in HR+/HER2- breast cancer.

A Representative images from immunohistochemical staining of PTEN neddylation on K402 in tumors and matched adjacent tissues. Image J was used to perform Semi-quantitative analysis. Data were analyzed using Student's *t*-test. Scale bars, 50 μm. PTEN neddylation on K402 expression are shown as box plots. **B** Kaplan-Meier plot of overall survival of patients with breast carcinomas. A log-rank test was used to show differences between groups. **C** Representative images from immunohistochemical staining of neddylated PTEN on K402 in different breast cancer subtypes are shown. Scale bars, 50 μm. Data were analyzed using the one-way ANOVA test. PTEN neddylation on K402 expression are shown as box plots. **D** Representative images from immunohistochemical staining of PTEN and PTEN neddylation on K402 in liver metastasis of breast cancer and preinvasive carcinoma tissues and adjacent tissues. Scale bars, 100 μm. **E-H** The MMTV-*PyMT* Palbociclib resistant mouse model (n=3) was established by Palbociclib (75mg/kg) gavage daily for 35 days. The Palbociclib sensitive group administered Palbociclib (75mg/kg) by gavage daily for 20 days (**E**). The breast tumors were removed and photographed (**F**). Tumors were isolated, volume (**H**) and their weights (**G**) were measured. Data are presented as means ± SD. **I** Representative images from immunohistochemical staining of PTEN and PTEN neddylation on K402 in control group, Palbo-S and Palbo-R tumors. Scale bar, 50 μm. **J** Immunoblot analysis of anti-PTEN immunoprecipitate from spontaneous breast tumors of MMTV-*PyMT* mice in three groups. **K** IC50 of Palbociclib-resistant MMTV-*PyMT* breast tumor cells (MMTV-*PyMT*-Palbo-R) increased to 20.33 μM. MMTV-*PyMT*-Palbo-R and MMTV-*PyMT*-Palbo-S cells were seeded in 96-well plates in triplicates treated with increasing concentration of Palbociclib and then lysed for CCK8 assay. *P* values were calculated by Student's *t*-test. (**A, D**), one-way ANOVA test (**C, G, H, I)** and log-rank test (**B**). Error bars, ± SD. ns, not significant, *$P < 0.05$, **$P < 0.01$, ***$P < 0.001$.

Figure 2

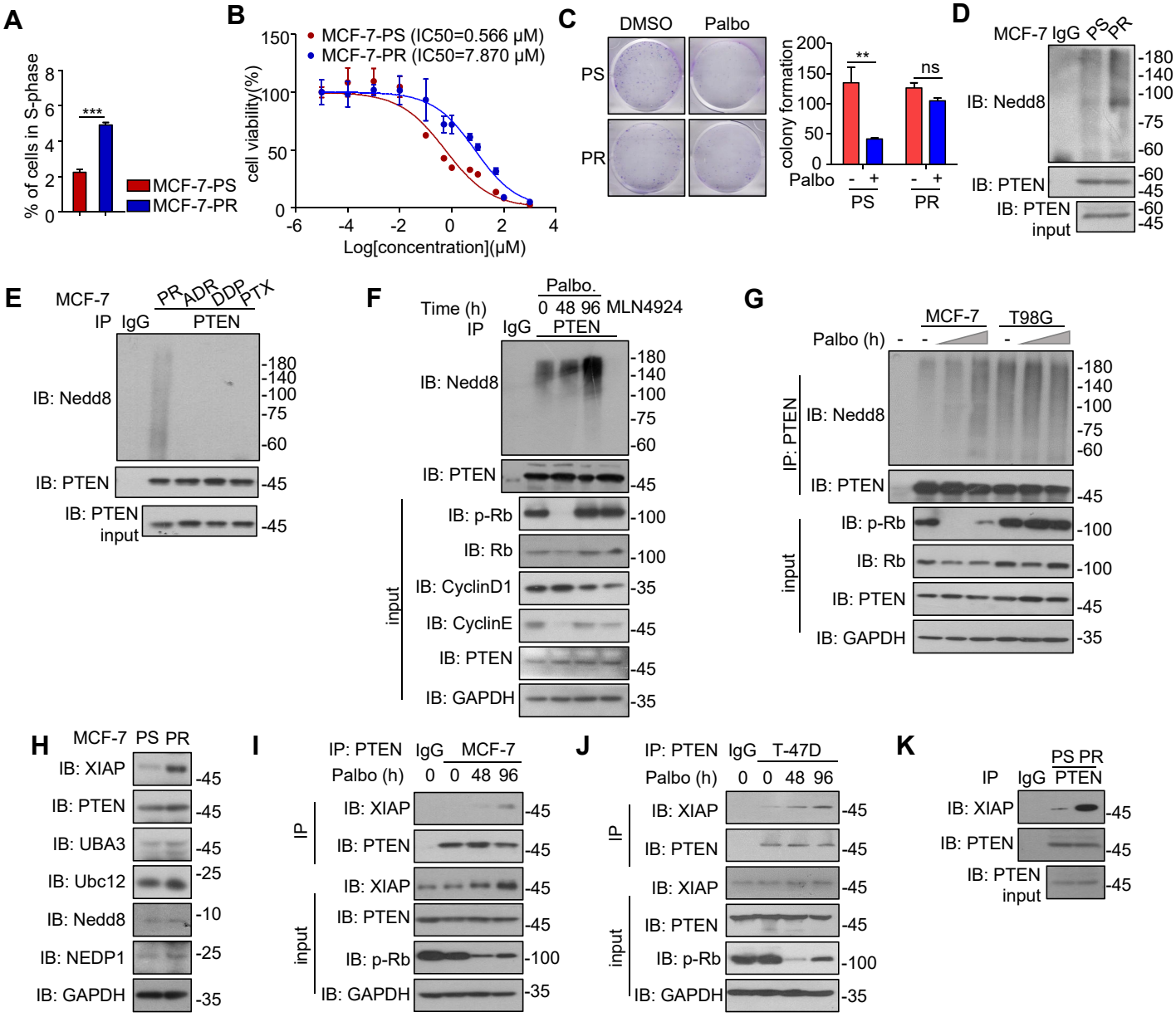
A
% of cells in S-phase
***
MCF-7-PS
MCF-7-PR
B
MCF-7-PS (IC50=0.566 μM)
MCF-7-PR (IC50=7.870 μM)
cell viability(%)
Log[concentration](μM)
C
DMSO
Palbo
PS
PR
colony formation
**
ns
Palbo
PS
PR
D
MCF-7 IgG PS PR
IB: Nedd8
IB: PTEN
IB: PTEN input
E
MCF-7
PR ADR DDP PTX
IP IgG PTEN
IB: Nedd8
IB: PTEN
IB: PTEN input
F
Palbo.
Time (h) 0 48 96 MLN4924
IP IgG PTEN
IB: Nedd8
IB: PTEN
input
IB: p-Rb
IB: Rb
IB: CyclinD1
IB: CyclinE
IB: PTEN
IB: GAPDH
G
MCF-7 T98G
Palbo (h)
IP: PTEN
IB: Nedd8
IB: PTEN
input
IB: p-Rb
IB: Rb
IB: PTEN
IB: GAPDH
H
MCF-7 PS PR
IB: XIAP
IB: PTEN
IB: UBA3
IB: Ubc12
IB: Nedd8
IB: NEDP1
IB: GAPDH
I
IP: PTEN IgG MCF-7
Palbo (h) 0 0 48 96
IP
IB: XIAP
IB: PTEN
input
IB: XIAP
IB: PTEN
IB: p-Rb
IB: GAPDH
J
IP: PTEN IgG T-47D
Palbo (h) 0 0 48 96
IP
IB: XIAP
IB: PTEN
input
IB: XIAP
IB: PTEN
IB: p-Rb
IB: GAPDH
K
PS PR
IP IgG PTEN
IB: XIAP
IB: PTEN
IB: PTEN input

Figure 2 High protein level of XIAP enhances the PTEN neddylation in Palbociclib resistant breast cancer.

A Cell-cycle analysis was performed in MCF-7-PS and MCF-7-PR cells. The percentage of cells in S-phase is depicted. Data are presented as the mean ± SD (n = 3). **B** IC50 of PR cells (MCF-7-PR) increased to 7.87 μM. MCF-7-PR and MCF-7-PS cells were seeded in 96-well plates in triplicates and then treated with Palbociclib and then lysed for CCK8 assay. **C** Colony formation assay was performed in the indicated cells and then treated with Palbociclib (0.1 μM, 15 days). Data are presented as means ± SD. Results are from a representative experiment performed in triplicate. Image J was used to perform quantitative analysis. **D** Immunoblot analysis of anti-PTEN immunoprecipitate from MCF-7-PS and MCF-7-PR cells. **E** Immunoblot analysis of anti-PTEN immunoprecipitate from MCF-7 drug resistant cells including MCF-7-PR, MCF-7-ADR, MCF-7-DDP, MCF-7-PTX. **F** Immunoblot analysis of anti-PTEN immunoprecipitate from early adaptative resistant MCF-7 cells treated with Palbociclib (0.5 μM, 0 h/48 h/96 h) and MLN4924 (1 μM, 12 h). **G** Immunoblot analysis of anti-PTEN immunoprecipitate from early adaptative resistant MCF-7 cells and T98G cells. **H** Immunoblot of WCL from MCF-7-PS and MCF-7-PR cells. **I-K** Immunoblot analysis of anti-PTEN immunoprecipitate and WCL from early adaptative Palbociclib resistance in MCF-7 (**I**) and T-47D (**J**) and acquired Palbociclib-resistant MCF-7 cells (**K**). *P* values were calculated by Student's *t*-test. (**A**), one-way ANOVA test (**C**). Error bars, ± SD. ns, not significant, $^{*}P < 0.05$, $^{**}P < 0.01$, $^{***}P < 0.001$.

Figure 3

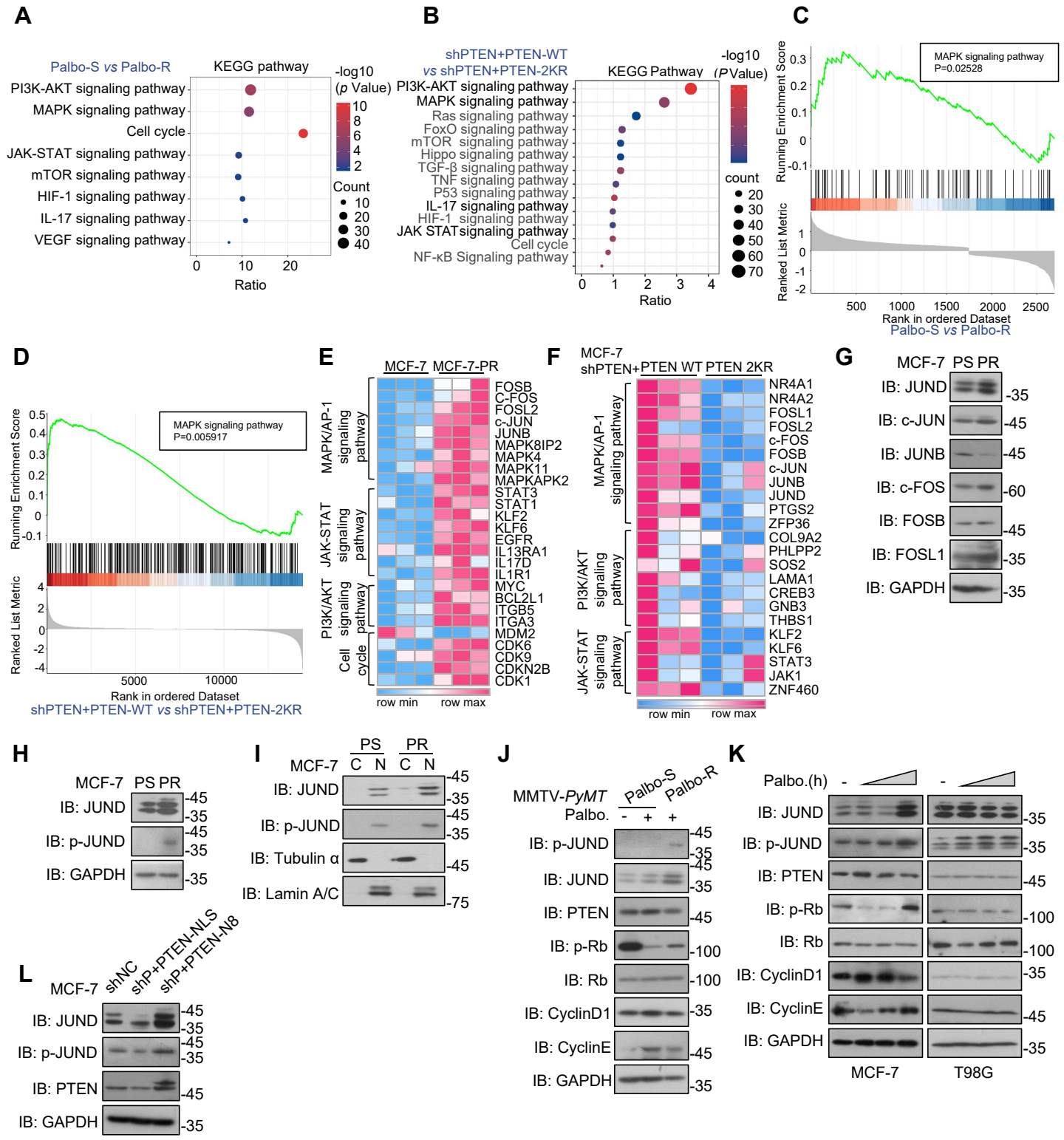
A
Palbo-S vs Palbo-R
KEGG pathway
PI3K-AKT signaling pathway
MAPK signaling pathway
Cell cycle
JAK-STAT signaling pathway
mTOR signaling pathway
HIF-1 signaling pathway
IL-17 signaling pathway
VEGF signaling pathway
-log10 (p Value)
Count
Ratio
B
shPTEN+PTEN-WT vs shPTEN+PTEN-2KR
KEGG Pathway
PI3K-AKT signaling pathway
MAPK signaling pathway
Ras signaling pathway
FoxO signaling pathway
mTOR signaling pathway
Hippo signaling pathway
TGF-β signaling pathway
TNF signaling pathway
P53 signaling pathway
IL-17 signaling pathway
HIF-1 signaling pathway
JAK STAT signaling pathway
Cell cycle
NF-κB Signaling pathway
-log10 (P Value)
count
Ratio
C
MAPK signaling pathway
P=0.02528
Running Enrichment Score
Ranked List Metric
Rank in ordered Dataset
Palbo-S vs Palbo-R
D
MAPK signaling pathway
P=0.005917
Running Enrichment Score
Ranked List Metric
Rank in ordered Dataset
shPTEN+PTEN-WT vs shPTEN+PTEN-2KR
E
MCF-7 MCF-7-PR
MAPK/AP-1 signaling pathway
JAK-STAT signaling pathway
PI3K/AKT signaling pathway
Cell cycle
FOSB
C-FOS
FOSL2
c-JUN
JUNB
MAPK8IP2
MAPK4
MAPK11
MAPKAPK2
STAT3
STAT1
KLF2
KLF6
EGFR
IL13RA1
IL17D
IL1R1
MYC
BCL2L1
ITGB5
ITGA3
MDM2
CDK6
CDK9
CDKN2B
CDK1
row min
row max
F
MCF-7
shPTEN+PTEN WT PTEN 2KR
MAPK/AP-1 signaling pathway
PI3K/AKT signaling pathway
JAK-STAT signaling pathway
NR4A1
NR4A2
FOSL1
FOSL2
c-FOS
FOSB
c-JUN
JUNB
JUND
PTGS2
ZFP36
COL9A2
PHLPP2
SOS2
LAMA1
CREB3
GNB3
THBS1
KLF2
KLF6
STAT3
JAK1
ZNF460
row min
row max
G
MCF-7 PS PR
IB: JUND
IB: c-JUN
IB: JUNB
IB: c-FOS
IB: FOSB
IB: FOSL1
IB: GAPDH
H
MCF-7 PS PR
IB: JUND
IB: p-JUND
IB: GAPDH
I
PS PR
MCF-7 C N C N
IB: JUND
IB: p-JUND
IB: Tubulin α
IB: Lamin A/C
J
MMTV-PyMT Palbo-S Palbo-R
Palbo. - + +
IB: p-JUND
IB: JUND
IB: PTEN
IB: p-Rb
IB: Rb
IB: CyclinD1
IB: CyclinE
IB: GAPDH
K
Palbo.(h) - -
IB: JUND
IB: p-JUND
IB: PTEN
IB: p-Rb
IB: Rb
IB: CyclinD1
IB: CyclinE
IB: GAPDH
MCF-7 T98G
L
MCF-7 shNC shP+PTEN-NLS shP+PTEN-N8
IB: JUND
IB: p-JUND
IB: PTEN
IB: GAPDH

Figure 3 PTEN neddylation enhances AP-1/JUND stability to promote Palbociclib resistance.

A, B The bubble charts depict the top ranked pathway analyzed from the KEGG pathway database. Enriched KEGG pathways were identified, which included upregulated or downregulated genes modulated by MCF-7-PR cells (**A**) and MCF-7 cells harboring a PTEN neddylation mutation (**B**). **C, D** GSEA plots of the indicated MCF-7 cells**. E** Heat map of the downstream or upstream target genes between the MCF-7-PS and MCF-7-PR cells. **F** Heat map of the downstream or upstream target genes between the MCF-7 shPTEN+PTEN-WT and MCF-7 shPTEN+PTEN-2KR cells. **G, H** Immunoblot of WCL from acquired Palbociclib-resistant or Palbociclb-sensetive MCF-7 cells **I** Immunoblot of JUND from nuclear and cytoplasmic fractionation of indicated cells. **J-L** Immunoblot of WCL from indicated cells.

Figure 4

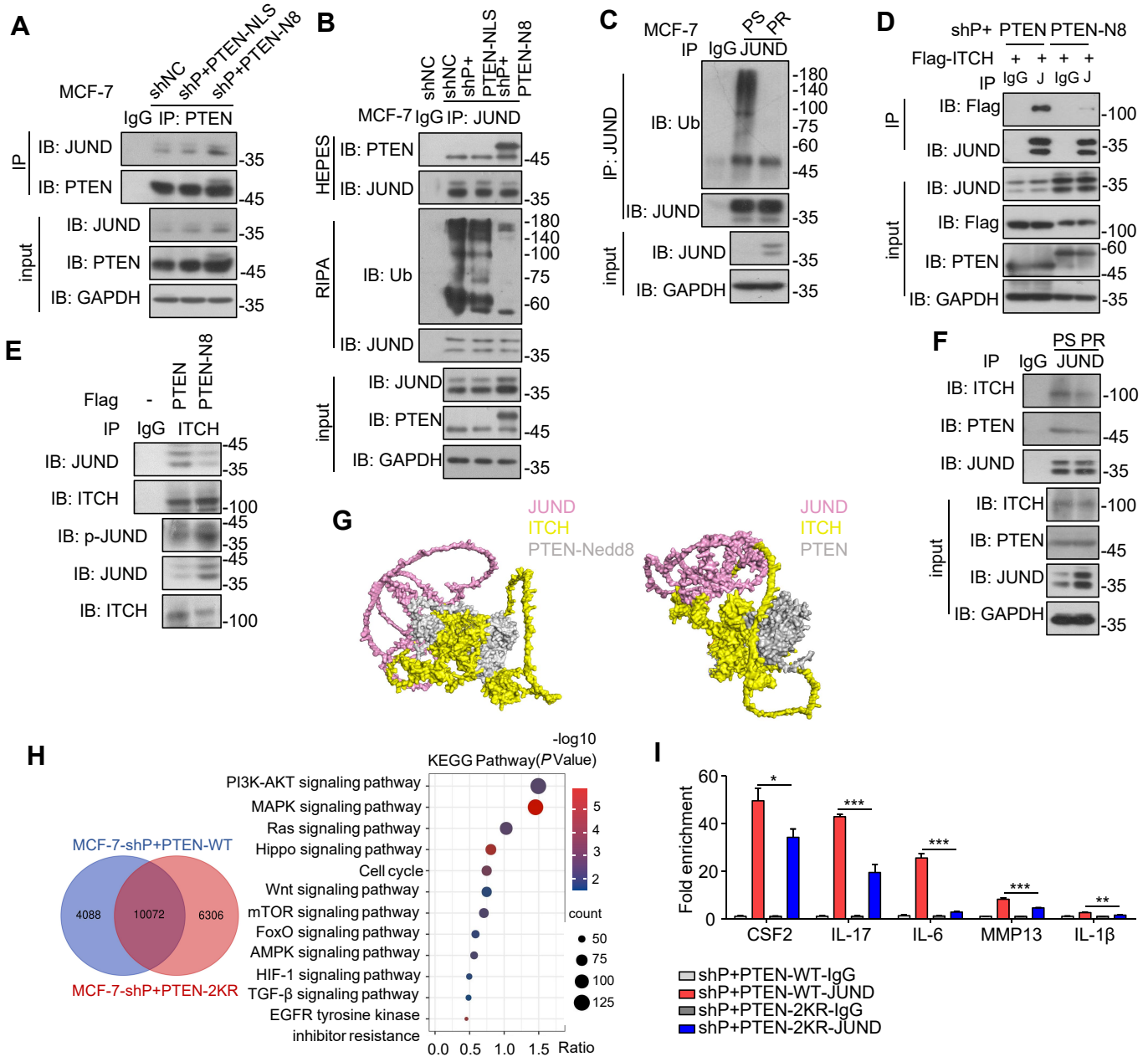
A
MCF-7
shNC
shP+PTEN-NLS
shP+PTEN-N8
IgG IP: PTEN
IP
IB: JUND
IB: PTEN
input
IB: JUND
IB: PTEN
IB: GAPDH
B
shNC
shNC
shP+
PTEN-NLS
shP+
PTEN-N8
MCF-7 IgG IP: JUND
HEPES
IB: PTEN
IB: JUND
RIPA
IB: Ub
IB: JUND
input
IB: JUND
IB: PTEN
IB: GAPDH
C
MCF-7
PS PR
IP IgG JUND
IP: JUND
IB: Ub
IB: JUND
input
IB: JUND
IB: GAPDH
D
shP+ PTEN PTEN-N8
Flag-ITCH + + + +
IP IgG J IgG J
IP
IB: Flag
IB: JUND
input
IB: JUND
IB: Flag
IB: PTEN
IB: GAPDH
E
Flag - PTEN PTEN-N8
IP IgG ITCH
IB: JUND
IB: ITCH
IB: p-JUND
IB: JUND
IB: ITCH
F
PS PR
IP IgG JUND
IB: ITCH
IB: PTEN
IB: JUND
input
IB: ITCH
IB: PTEN
IB: JUND
IB: GAPDH
G
JUND
ITCH
PTEN-Nedd8
JUND
ITCH
PTEN
H
MCF-7-shP+PTEN-WT
4088
10072
6306
MCF-7-shP+PTEN-2KR
-log10
KEGG Pathway(PValue)
PI3K-AKT signaling pathway
MAPK signaling pathway
Ras signaling pathway
Hippo signaling pathway
Cell cycle
Wnt signaling pathway
mTOR signaling pathway
FoxO signaling pathway
AMPK signaling pathway
HIF-1 signaling pathway
TGF-β signaling pathway
EGFR tyrosine kinase inhibitor resistance
count
Ratio
I
Fold enrichment
CSF2
IL-17
IL-6
MMP13
IL-1β
shP+PTEN-WT-IgG
shP+PTEN-WT-JUND
shP+PTEN-2KR-IgG
shP+PTEN-2KR-JUND

Figure 4 PTEN neddylation decreases JUND ubiquitination.

A Immunoblot analysis of anti-PTEN immunoprecipitate from the indicated cells. **B, C, D, F** Immunoblot analysis of anti-JUND immunoprecipitate from the indicated cells. **E** Immunoblot analysis of anti-ITCH immunoprecipitate from the indicated cells. **G** Structure simulation of ITCH (yellow), JUND (pink) and PTEN or PTEN-Nedd8 (grey) by AlphaFold2.0. **H** Venn diagram of overlapping promoters bound by JUND in MCF-7 shP+PTEN-WT/2KR cells. Numbers represent the number of promoters targeted by the indicated proteins. A bubble chart of the enriched KEGG pathways comprising the 6306 target genes in MCF-7 shP+PTEN-2KR cells. **I** Verification of Cut＆Tag results using qPCR analysis of indicated genes in MCF-7 shP+PTEN-WT/2KR cells. Results are represented as fold change over control. *P* values were calculated by one-way ANOVA test. Error bars, ± SD. ns, not significant, $^{*}P < 0.05$, $^{**}P < 0.01$, $^{***}P < 0.001$.

Figure 5

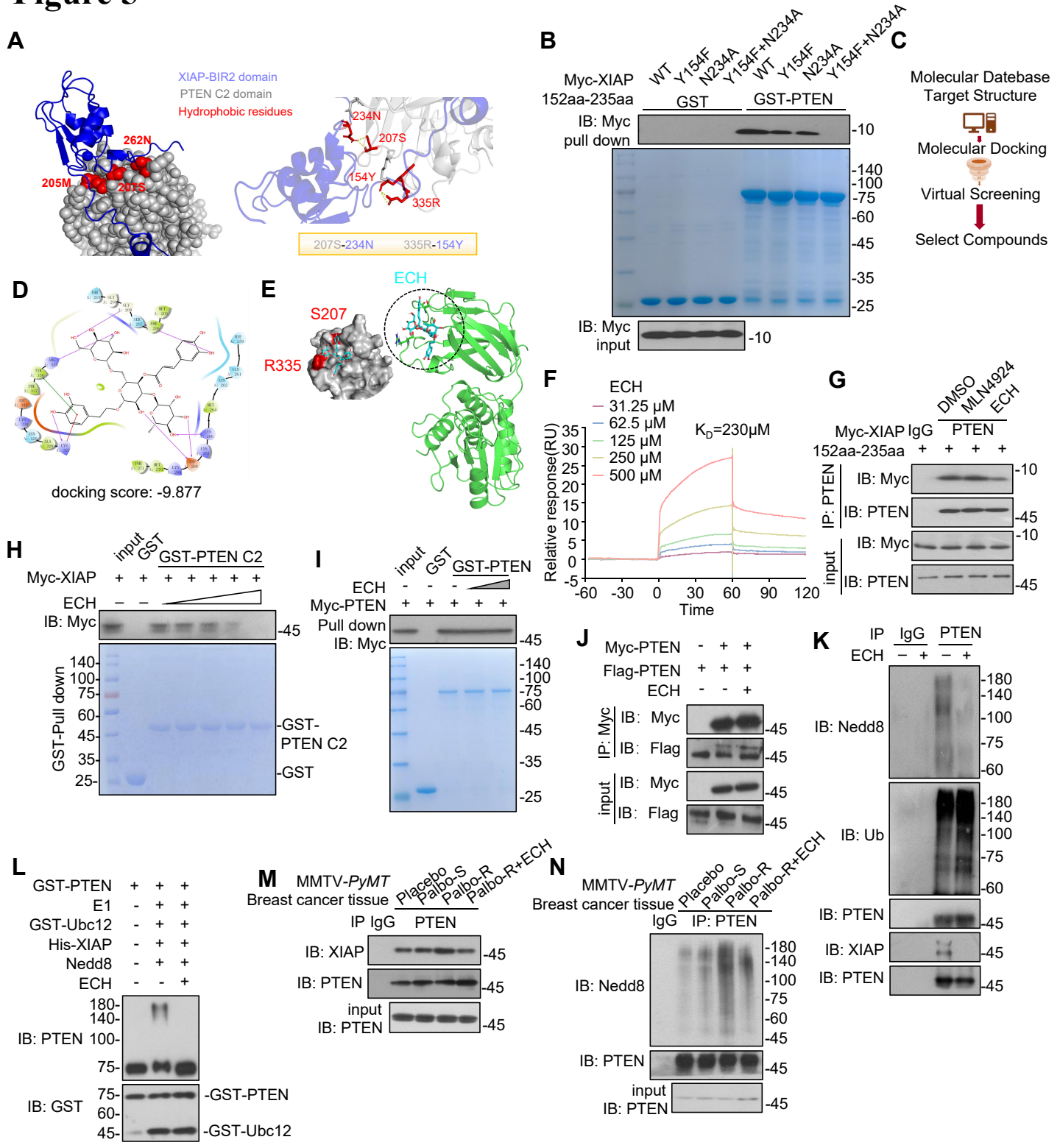
A
XIAP-BIR2 domain
PTEN C2 domain
Hydrophobic residues
262N
205M
207S
234N
207S
154Y
335R
207S-234N
335R-154Y
B
Myc-XIAP 152aa-235aa
WT
Y154F
N234A
Y154F+N234A
GST
GST-PTEN
IB: Myc pull down
IB: Myc input
C
Molecular Datebase Target Structure
Molecular Docking
Virtual Screening
Select Compounds
D
docking score: -9.877
E
ECH
S207
R335
F
ECH
31.25 μM
62.5 μM
125 μM
250 μM
500 μM
K_D=230μM
Relative response(RU)
Time
G
DMSO
MLN4924
ECH
Myc-XIAP 152aa-235aa
IgG
PTEN
IP: PTEN
IB: Myc
IB: PTEN
input
H
input
GST
GST-PTEN C2
Myc-XIAP
ECH
IB: Myc
GST-Pull down
GST-PTEN C2
GST
I
input
GST
GST-PTEN
ECH
Myc-PTEN
Pull down
IB: Myc
J
Myc-PTEN
Flag-PTEN
ECH
IP: Myc
IB: Myc
IB: Flag
input
K
IP
IgG
PTEN
ECH
IB: Nedd8
IB: Ub
IB: PTEN
IB: XIAP
L
GST-PTEN
E1
GST-Ubc12
His-XIAP
Nedd8
ECH
IB: PTEN
IB: GST
GST-PTEN
GST-Ubc12
M
MMTV-PyMT Breast cancer tissue
Placebo
Palbo-S
Palbo-R
Palbo-R+ECH
IP IgG
PTEN
IB: XIAP
IB: PTEN
input
N
MMTV-PyMT Breast cancer tissue
IgG
IP: PTEN
IB: Nedd8
IB: PTEN
input

Figure 5 Identification of Echinacoside as a PTEN neddylation inhibitor.

A Molecular docking of PTEN and XIAP. **B** GST pull-down assay of GST-tagged PTEN and Myc-tagged XIAP (152aa-235aa) WT and mutants in HEK-293T cells. **C** The workflow of virtual screening. **D**. Structural formula of Echinacoside. **E** Molecular docking of ECH and PTEN to estimate the binding ability**. F** ECH (31.25, 62.5, 125, 250, and 500 μM) exhibited dose-dependent binding to GST-tagged PTEN that was immobilized onto a CM5 sensor chip surface. **G, J** The immunoblot analysis using anti-PTEN antibodies (**G**) or anti-Myc antibodies (**J**) was performed, examining the immunoprecipitated proteins from HEK-293T cells transfected with the indicated constructs, as well as whole cell lysates (WCL). **H, I** GST pull-down assay of GST-tagged PTEN C2 (**H**) or WT (**I**) and Myc-tagged XIAP or PTEN in HEK-293T cells, which were treated with increasing concentration of ECH. **K, M, N** Immunoblot analysis of anti-PTEN immunoprecipitate and WCL from MCF-7 (**K**) and MMTV-*PyMT* breast cancer tissue (**M, N**). **L** *In vitro* neddylation of PTEN. His-XIAP and GST-PTEN proteins were incubated with Nedd8, Nedd8-E1, GST-Ubc12, ECH (10μg). Reactions were performed as described in the materials and methods section. Samples were analyzed by western blot with indicated antibodies.

Figure 6

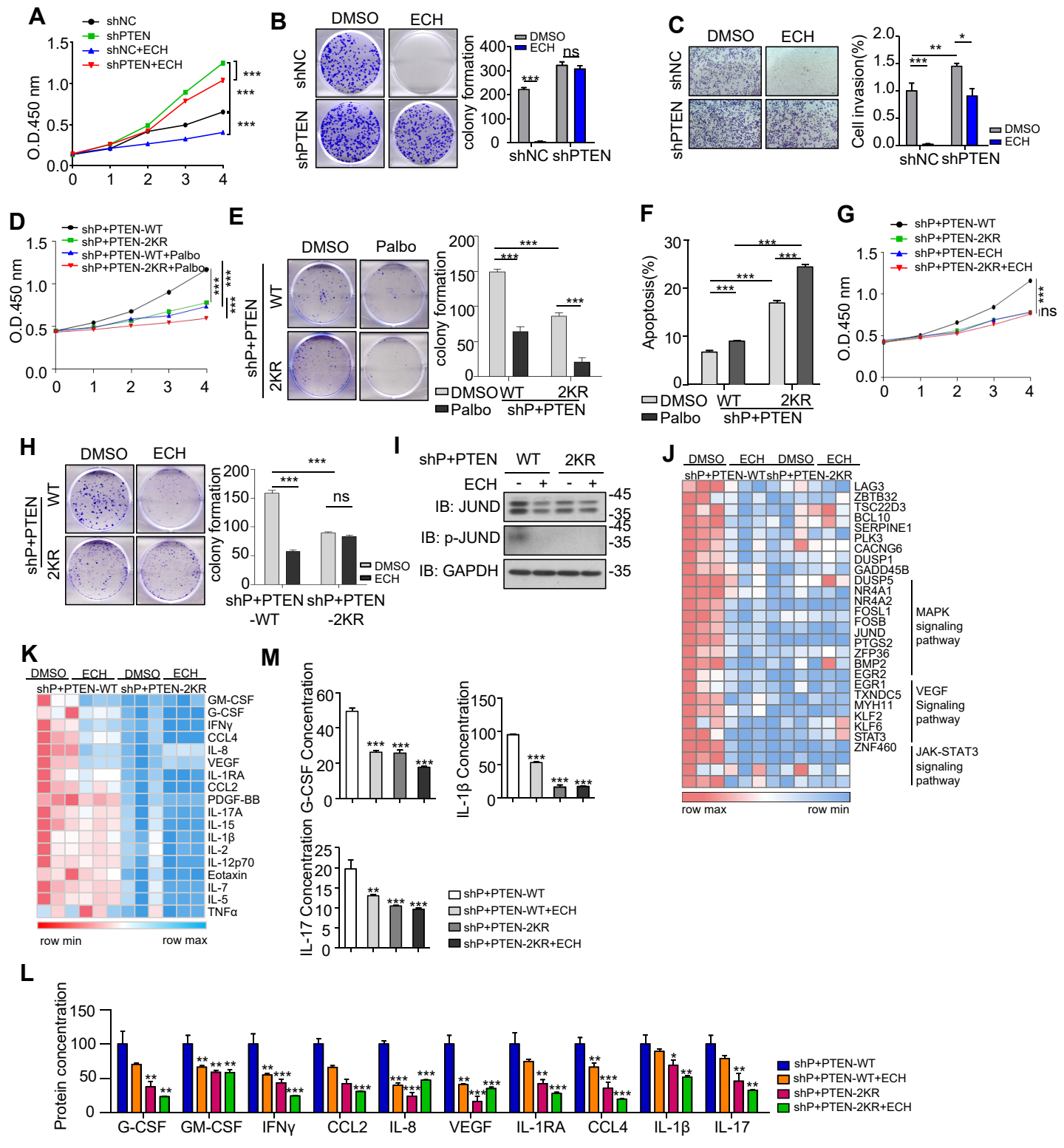
A
shNC
shPTEN
shNC+ECH
shPTEN+ECH
O.D.450 nm
B
DMSO
ECH
shNC
shPTEN
colony formation
ns
shNC shPTEN
C
Cell invasion(%)
D
shP+PTEN-WT
shP+PTEN-2KR
shP+PTEN-WT+Palbo
shP+PTEN-2KR+Palbo
E
Palbo
WT
2KR
shP+PTEN
F
Apoptosis(%)
G
shP+PTEN-ECH
shP+PTEN-2KR+ECH
H
I
IB: JUND
IB: p-JUND
IB: GAPDH
J
LAG3
ZBTB32
TSC22D3
BCL10
SERPINE1
PLK3
CACNG6
DUSP1
GADD45B
DUSP5
NR4A1
NR4A2
FOSL1
FOSB
JUND
PTGS2
ZFP36
BMP2
EGR2
EGR1
TXNDC5
MYH11
KLF2
KLF6
STAT3
ZNF460
MAPK signaling pathway
VEGF Signaling pathway
JAK-STAT3 signaling pathway
row max
row min
K
GM-CSF
G-CSF
IFNγ
CCL4
IL-8
VEGF
IL-1RA
CCL2
PDGF-BB
IL-17A
IL-15
IL-1β
IL-2
IL-12p70
Eotaxin
IL-7
IL-5
TNFα
M
G-CSF Concentration
IL-1β Concentration
IL-17 Concentration
shP+PTEN-WT
shP+PTEN-WT+ECH
shP+PTEN-2KR
shP+PTEN-2KR+ECH
L
Protein concentration
G-CSF
GM-CSF
IFNγ
CCL2
IL-8
VEGF
IL-1RA
CCL4
IL-1β
IL-17

Figure 6 ECH is dependent on PTEN neddylation to suppress tumorigenesis.

A CCK8 assay was performed in the indicated cells treated with ECH for 200 μM, 4 days. **B** Colony formation assay was performed in the indicated cells treated with ECH (200 μM,15 days). **C** Cell invasion assay was performed in the indicated cells treated with ECH (200 μM, 24h). **D** CCK8 assay was performed in the indicated cells treated with Palbociclib for 0.5 μM, 4 days. **E** Colony formation assay was performed in the indicated cells treated with Palbociclib for 0.1 μM, 15 days. **F** Cell apoptosis assay was performed in the indicated cells treated with Palbociclib for 0.5 μM, 24 hours. **G** Cell proliferation curve of ECH (200μM, 4 days) in MCF-7 shP+PTEN-WT/2KR cells by CCK8 assay. **H** Colony formation assay was performed in the indicated cells treated with ECH (200μM) for 15 days. **I** Immunoblot of WCL from the indicated cells treated by ECH (200μM, 24h). **J** The RNA sequencing-based heatmap analysis was executed to investigate the gene expression patterns in MCF-7 shPTEN+PTEN-WT and shPTEN+PTEN-2KR cells, either untreated or following exposure to ECH (200μM, 24h). **K** Cytometric bead array was performed to detect protein expression of the indicated cytokines. Heatmap was performed to exhibit protein expression in the indicated MCF-7 cells. The cells were treated with ECH for 200μM, 24h. **L** The protein level of G-CSF, GM-CSF, IFNγ, CCL2, IL-8, VEGF, IL-1RA, IL-1β, IL-17 and CCL4 from the immunoassay array of indicated cells are shown as bar chart. **M** G-CSF，IL-1β and IL-17 protein levels were measured in the indicated cells by Elisa. *P* values were calculated by one-way ANOVA test. (**A-H, L, M**). Error bars, ± SD. ns, not significant, **P* < 0.05, ***P* < 0.01, ****P* < 0.001.

Figure 7

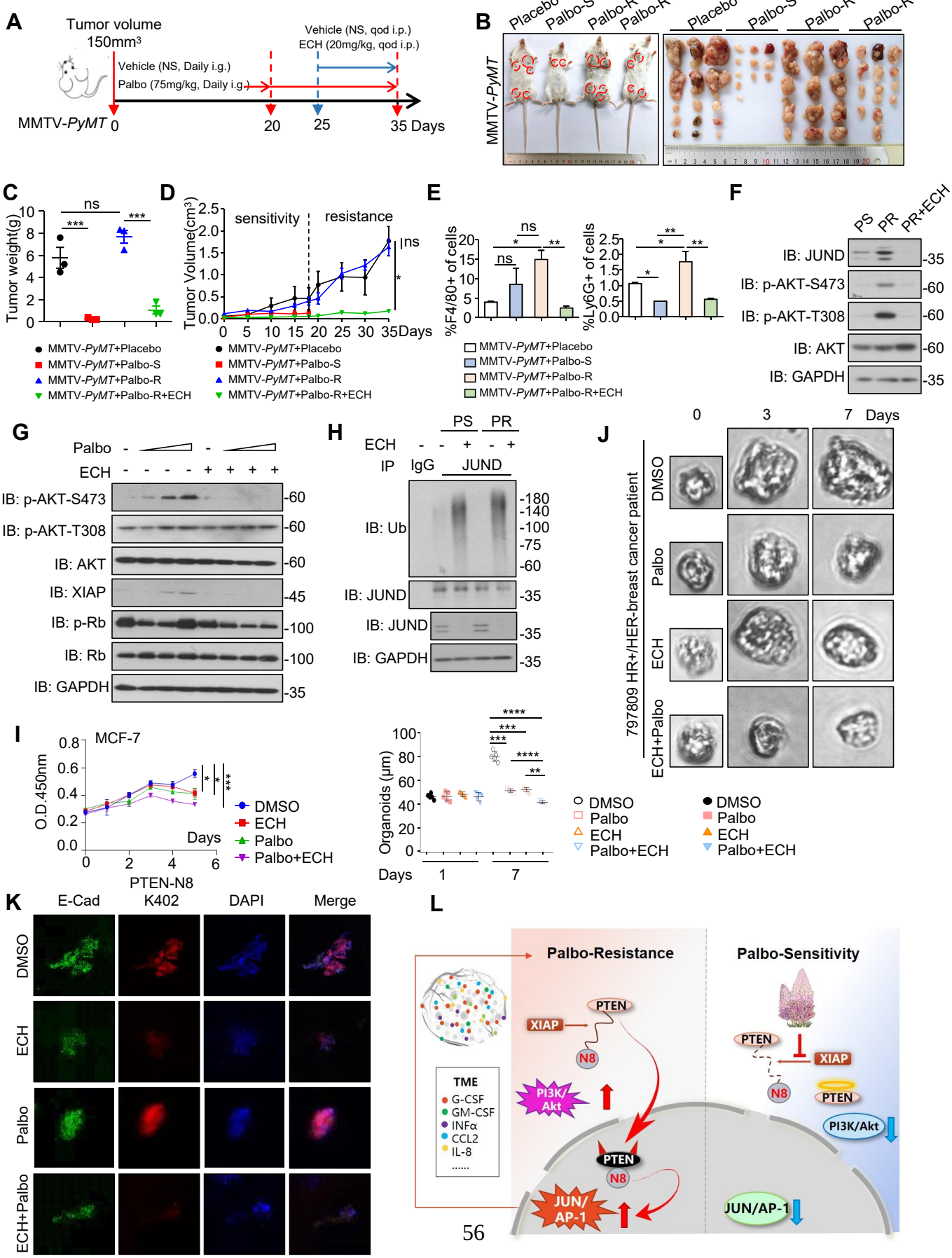
A
Tumor volume 150mm³
Vehicle (NS, Daily i.g.)
Palbo (75mg/kg, Daily i.g.)
Vehicle (NS, qod i.p.)
ECH (20mg/kg, qod i.p.)
MMTV-PyMT
0
20
25
35 Days
B
Placebo
Palbo-S
Palbo-R
Palbo-R+ECH
MMTV-PyMT
C
Tumor weight(g)
ns
***
MMTV-PyMT+Placebo
MMTV-PyMT+Palbo-S
MMTV-PyMT+Palbo-R
MMTV-PyMT+Palbo-R+ECH
D
Tumor Volume(cm³)
sensitivity
resistance
ns
*
Days
E
%F4/80+ of cells
%Ly6G+ of cells
ns
*
**
F
PS
PR
PR+ECH
IB: JUND
IB: p-AKT-S473
IB: p-AKT-T308
IB: AKT
IB: GAPDH
-35
-60
G
Palbo
ECH
IB: p-AKT-S473
IB: p-AKT-T308
IB: AKT
IB: XIAP
IB: p-Rb
IB: Rb
IB: GAPDH
-60
-45
-100
-35
H
PS
PR
ECH
IP
IgG
JUND
IB: Ub
IB: JUND
IB: GAPDH
-180
-140
-100
-75
-60
-35
I
MCF-7
O.D.450nm
Days
DMSO
ECH
Palbo
Palbo+ECH
PTEN-N8
Organoids (μm)
****
***
**
J
0
3
7
Days
797809 HR+/HER-breast cancer patient
DMSO
Palbo
ECH
ECH+Palbo
K
E-Cad
K402
DAPI
Merge
DMSO
ECH
Palbo
ECH+Palbo
L
Palbo-Resistance
Palbo-Sensitivity
PTEN
XIAP
N8
PI3K/Akt
TME
G-CSF
GM-CSF
INFα
CCL2
IL-8
.....
JUN/AP-1

Figure 7 Combination ECH enhances the sensitivity of Palbociclib in HR+/HER2-breast cancer.

A-D The MMTV-*PyMT* Palbociclib resistant mouse model (n=3) was established by Palbociclib (75mg/kg, i.g.) daily for 35 days. ECH (20mg/kg, i.p.) was daily treated for 10 days. The breast tumors were removed and photographed (**B**). Tumors were isolated, volume (**D**) and their weights (**C**) were measured. Data are presented as means ± SD. **E** The F4/80$^+$, Ly6G$^+$ labelled cells derived from the breast tumors of MMTV-*PyMT* placebo, Palbo-S, Palbo-R, Palbo-R+ECH mice, were isolated and calculated by flow cytometry sorting. Data are shown as mean ± SD and analyzed by a one-way ANOVA test. ns, not significant, *$P < 0.05$, **$P < 0.01$, ***$P < 0.001$. **F** Immunoblot of WCL from the indicated cells treated with Palbociclib (0.5 μM, 24h/96h) and ECH (200μM, 96h). **G** Immunoblot of WCL from the indicated cells treated with Palbociclib (0.5 μM, 0h/24h/72h/96h) and ECH (200 μM, 0h/24h/72h/96h). **H** Immunoblot analysis of anti-JUND immunoprecipitate and WCL in MCF-7 PS and PR cells. **I** CCK8 assay was performed in MCF-7 cells treated with Palbociclib (0.5 μM, 5 days) and ECH (200 μM, 5 days). **J** Representative images of HR+/HER2- breast cancer organoids derived from patient. ECH (200 μM) was daily treated for 7 days. Palbociclib (0.5 μM) was daily treated for 7 days. The diameter of organoids is shown as scatter diagram. *P* values were calculated by one-way ANOVA test. Error bars, ± SD. ns, not significant, *$P < 0.05$, **$P < 0.01$, ***$P < 0.001$. **K** Immunofluorescent of E-Cadherin (green) and neddylated PTEN (K402) (red) in breast cancer organoids. **L** Working model for PTEN neddylation in regulating CDK4/6 inhibitor resistance.